

Renewal models and coseismic stress transfer in the Corinth Gulf, Greece, fault system

Rodolfo Console,^{1,2} Giuseppe Falcone,¹ Vassilis Karakostas,³ Maura Murru,¹ Eleftheria Papadimitriou,³ and David Rhoades⁴

Received 27 November 2012; revised 25 June 2013; accepted 1 July 2013; published 30 July 2013.

[1] We model interevent times and Coulomb static stress transfer on the rupture segments along the Corinth Gulf extension zone, a region with a wealth of observations on strong-earthquake recurrence behavior. From the available information on past seismic activity, we have identified eight segments without significant overlapping that are aligned along the southern boundary of the Corinth rift. We aim to test if strong earthquakes on these segments are characterized by some kind of time-predictable behavior, rather than by complete randomness. The rationale for time-predictable behavior is based on the characteristic earthquake hypothesis, the necessary ingredients of which are a known faulting geometry and slip rate. The tectonic loading rate is characterized by slip of 6 mm/yr on the westernmost fault segment, diminishing to 4 mm/yr on the easternmost segment, based on the most reliable geodetic data. In this study, we employ statistical and physical modeling to account for stress transfer among these fault segments. The statistical modeling is based on the definition of a probability density distribution of the interevent times for each segment. Both the Brownian Passage-Time (BPT) and Weibull distributions are tested. The time-dependent hazard rate thus obtained is then modified by the inclusion of a permanent physical effect due to the Coulomb static stress change caused by failure of neighboring faults since the latest characteristic earthquake on the fault of interest. The validity of the renewal model is assessed retrospectively, using the data of the last 300 years, by comparison with a plain time-independent Poisson model, by means of statistical tools including the Relative Operating Characteristic diagram, the R-score, the probability gain and the log-likelihood ratio. We treat the uncertainties in the parameters of each examined fault source, such as linear dimensions, depth of the fault center, focal mechanism, recurrence time, coseismic slip, and aperiodicity of the statistical distribution, by a Monte Carlo technique. The Monte Carlo samples for all these parameters are drawn from a uniform distribution within their uncertainty limits. We find that the BPT and the Weibull renewal models yield comparable results, and both of them perform significantly better than the Poisson hypothesis. No clear performance enhancement is achieved by the introduction of the Coulomb static stress change into the renewal model.

Citation: Console, R., G. Falcone, V. Karakostas, M. Murru, E. Papadimitriou, and D. Rhoades (2013), Renewal models and coseismic stress transfer in the Corinth Gulf, Greece, fault system, *J. Geophys. Res. Solid Earth*, 118, 3655–3673, doi:10.1002/jgrb.50277.

1. Introduction

[2] Crustal movement within the Aegean region is accommodated by slip on a large number of mapped faults, and probably also on many unmapped ones. The deformation is concentrated on a few narrow, more intensely deforming

zones, for example the Gulf of Corinth (denoted by the yellow rectangle in Figure 1), which is one of intense seismic activities, mostly associated with faulting and crustal extension. The Gulf has the general shape of an asymmetric half-graben with the southern footwall being uplifted [Roberts and Jackson, 1991; Armijo *et al.*, 1996]. The western end of the Gulf of Corinth is connected through the Rio-Antirrio strait to the Gulf of Patras, which does not have any major faults comparable to those affecting the Gulf of Corinth. The eastern part of the Gulf of Corinth truncates the Megara basin through a complex pattern of faults with a more NE-SW strike [Leeder *et al.*, 1991]. Faults also affect the deepest part of the Gulf, which is located underwater [Brooks and Ferentinos, 1984].

[3] The deformation of the Gulf of Corinth has been measured by comparing GPS measurements with old triangulations

¹Istituto Nazionale di Geofisica e Vulcanologia, Rome, Italy.

²Center of Integrated Geomorphology for the Mediterranean Area, Potenza, Italy.

³Geophysics Department, Aristotle University of Thessaloniki, Thessaloniki, Greece.

⁴GNS Science, Lower Hutt, New Zealand.

Corresponding author: M. Murru, Istituto Nazionale di Geofisica e Vulcanologia, Rome 00143, Italy. (maura.murru@ingv.it)

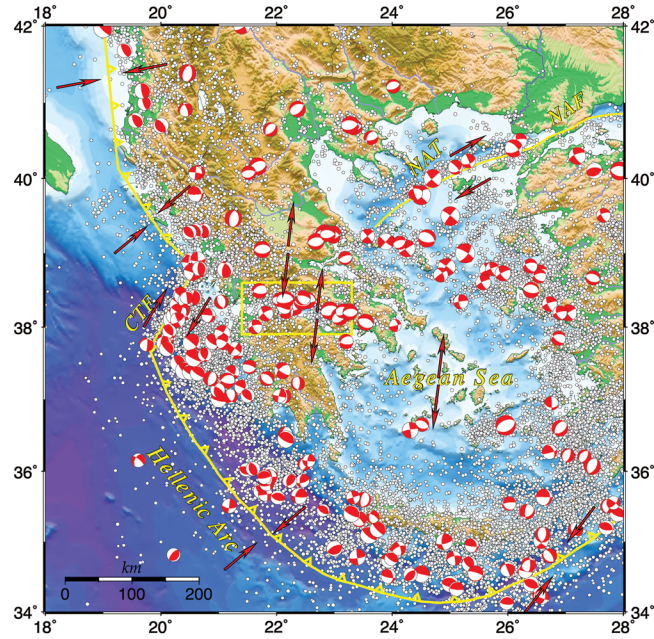


Figure 1. Main structures, spatial distribution of the earthquakes with $M \geq 4.0$ since 1964, and available focal mechanisms during the last five decades in the region of Greece and Aegean Sea. The arrows indicate the different kinematics (contractional, strike-slip, and extensional) that dominates in the region. The study area is shown by a yellow rectangle. CTF: Cephalonia Transform Fault, NAT: North Aegean Trough, NAF: North Anatolian Fault.

conducted in 1890 or between 1966 and 1972 [Billiris *et al.*, 1991; Clarke *et al.*, 1997; Davies *et al.*, 1997; Briole *et al.*, 2000]. The geodetically measured N-S extension is about 15 mm/yr in the western part of the Gulf around Rio, and about 10 mm/yr in the eastern part of the Gulf, around Corinth. A comparison between several GPS surveys measured over shorter duration gives slightly higher values, but with the same difference between the western and eastern ends of the Gulf. It therefore seems clear that the present deformation is faster around Rio than around Corinth. This deformation is relatively well confined in the center of the Gulf on a very narrow deforming zone.

[4] Information on the strong earthquakes in the Corinth Gulf, both historical and instrumental, is provided by Ambraseys and Jackson [1990, 1997], Papazachos and Papazachou [2003], Ambraseys [2009], and the regional catalog compiled at the Geophysics Department of Aristotle University of Thessaloniki (<http://geophysics.geo.auth.gr/ss/>). Grunthal and Wahlstrom [2007] compiled a unified database of large earthquakes ($M_w \geq 6.0$) taken from local earthquake catalogs for all of Europe and the near surrounding seas, among which the catalogs compiled by Papazachos and Papazachou [2003] are included. They considered the catalog completeness for the Greek and surrounding areas, for $M_w \geq 6.0$ and $M_w \geq 7.0$ since about 1850 and since about 1500, respectively. For the scope of our work, we prefer using the above cited catalogs, as they are well documented.

[5] We considered all the events with $M_w \geq 6.0$ reported in these catalogs [i.e., Ambraseys and Jackson, 1990, 1997; Papazachos and Papazachou, 2003, and the regional catalog compiled at the Geophysics Department of Aristotle University of Thessaloniki] as characteristic, and, independently of their epicentral uncertainties, we may assume that

they are associated with certain fault segments along the Corinth Gulf. The temporal distribution of these events is shown in Figure 2, evidencing that they are not regularly distributed in time (Figure 2a), suggesting that there are “missing” events at least until 1700 AD. After 1700 AD, although earthquakes tend to occur in clusters, their number is rather constant through time (Figure 2b). This suggestion is confirmed by the cumulative distribution shown in Figure 3, which shows a sharp increase in the rate of occurrence for events reported after 1700 AD. Based on the

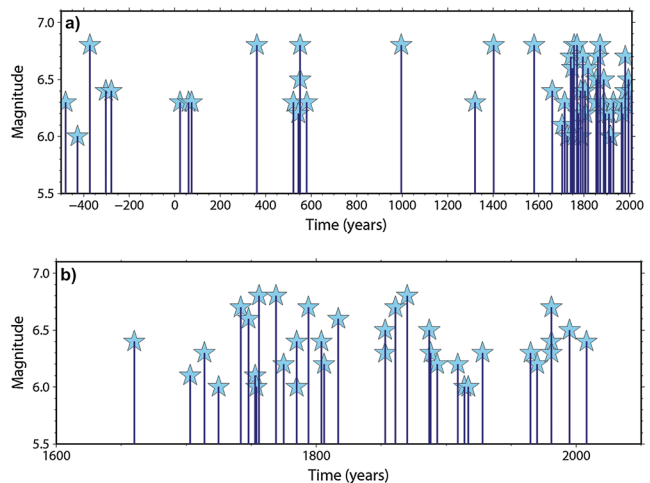


Figure 2. (a) Temporal distribution of the known earthquakes with $M_w \geq 6.0$ that were reported by Papazachos and Papazachou [2003] and occurred inside the rectangle of Figure 1. (b) As as in Figure 2a but for the period 1600–2010 AD.

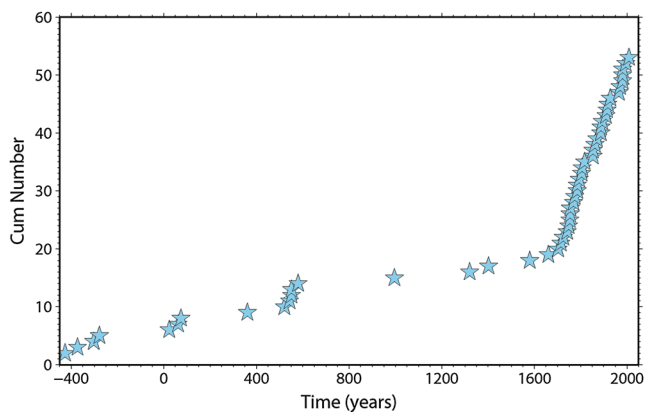


Figure 3. Cumulative occurrence rate of the earthquakes shown in Figure 2a.

approximate linearity of the plot from 1700 AD on, we assume our data to be complete for magnitudes $M_w \geq 6.0$, from 1700 AD to the present.

[6] In the Gulf of Corinth, the largest magnitude observed since 1700 AD is not greater than 6.8, and the strongest earthquake ever reported is hardly any greater, probably reflecting the lack of continuity of faults [Roberts and Jackson, 1991]. Most of the determined focal mechanisms of strong events indicate normal faulting with an N-S trending extension [Jackson, 1987; Taymaz et al., 1991; Hatzfeld et al., 1996; Bernard et al., 1997; Baker et al., 1997], and this is consistent with microearthquake mechanisms [Hatzfeld et al., 1990, 2000; Rigo et al., 1996]. Usually, the dimensions along the strike of normal faults do not exceed 20–25 km [Jackson and White, 1989], which implies an upper limit for the magnitude of the earthquakes that can occur on an individual fault segment. However, it is not clear whether the discontinuities separating the different segments are stable and will never break, or whether a rupture can occasionally jump from one segment to another, thereby leading to an earthquake of

greater magnitude [Jackson and White, 1989; Hatzfeld et al., 2000].

[7] We are aware that the hypothesis of characteristic ruptures adopted in this study is causing lively debates. Kagan et al. [2012] put in evidence that the “seismic gap” model sends a false message of relative safety. It implies that in the aftermath of a characteristic earthquake, a region is immune from further large shocks. But comprehensive studies [e.g., Kagan and Jackson, 1999] show that large earthquakes increase the probability at all magnitudes. Moreover, the characteristic earthquake model has not survived statistical testing. As far as they know, neither this model nor the seismic cycle model (which depends entirely on the “characteristic” assumption) is being tested in the Collaboratory for the Study of Earthquake Predictability centers in California, Japan, Switzerland, and New Zealand. A problem for testing these models is that they often address limited regions in which definitive earthquakes may not occur for centuries. The characteristic hypothesis is accepted by a few authors only in the early stages of fault system evolution when fault segments are still isolated from each other and the lateral terminations of footwall mountains and hanging wall basins coincide [Roberts, 1996 and references therein]. This allows one to define the length of fault segments by which to infer the lengths and positions of future ruptures. On the contrary, cumulative uplift/subsidence patterns become complex when normal faults grow, link, and interact.

[8] The aim of this study is to assess if a time-predictable model based on the characteristic earthquake hypothesis (like the Brownian Passage-Time (BPT) or the Weibull distribution) is suitable for the interevent times of the strong ($M \geq 6.0$) earthquakes observed in the study area, and if the forecasts obtained from this model perform better than those from a plain time-independent model. In other words, we want to test if some predictability exists for the time of occurrence of earthquakes larger than moment magnitude 6.0 in the Corinth Gulf. We also aim to test if the spatial and temporal distribution of earthquakes occurring on

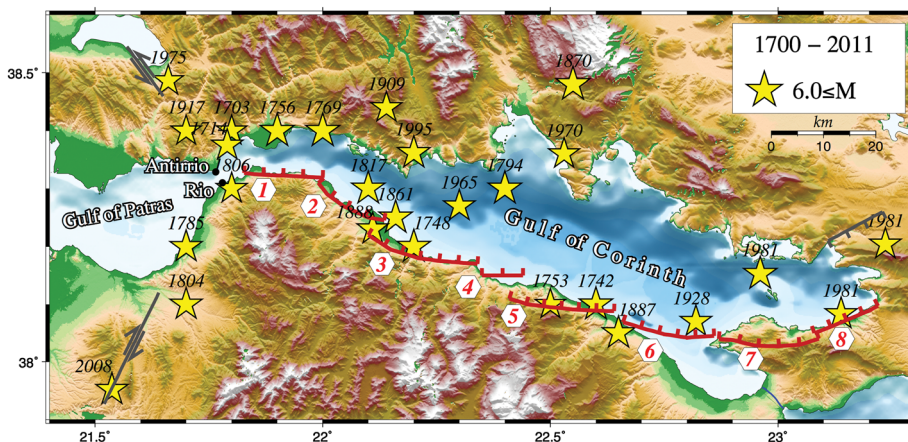


Figure 4. Tectonic map of the study area showing surface traces of the major fault segments of the Corinth area. The eight fault segments adopted for modeling the seismogenic structure following the southern bound of the Corinth rift are: 1 - Psathopyrgos, 2 - Aigion, 3 - Eliki, 4 - Offshore Akrata, 5 - Xylokaastro, 6 - Offshore Perachora, 7 - Skinos, and 8 - Aelpochori. Stars show the epicenters of the earthquakes of magnitude exceeding 6.0 and occurred after 1700 AD, as taken from Papazachos and Papazachou [2003]. The Trichonida, Kapareli, and Achaia faults edging the Corinth Gulf, with the respective associated events (1975, M_w 6.0, 1981, M_w 6.3, and 2008, M_w 6.4), are also shown in gray.

Table 1. Parameters of Fault Segments, Along the Southern Bound of Corinth Gulf, Considered in This Study^a

Segment Number	Segment Name	Length (km)	Width (km)	M_{max}	Coseismic Slip (m)	Slip Rate (mm/yr)	Historical Events Date/M	Recurrence Time
1	Psathopyrgos	15 ¹ 15±2 ² 15–20 ³	10 ¹	6.5 ²	0.75 ¹ 0.4–1.7 ²	6 ¹ 6 ²	July 29, 1714/6.2 ^{1,4} 6.3 ⁵ January 24, 1806/6.5 ⁴ 6.2 ^{1,5}	126 ¹
2	Aigion	16 ¹ 10±1 ² 8–14 ⁶	10 ¹	6.6 ⁶	0.88 ¹ 0.87 ⁷ 0.4–0.7 ⁶	6 ¹ 6.3 ⁶	May 25, 1748/ 6.6 ^{1,8} August 23, 1817 6.6 ^{1,4,5} September 9, 1888 6.3 ^{1,8} June 15, 1995 6.4 ^{1,7}	146 ¹ 120±20 ⁸ 320–640 ⁵ 242±60 ⁹
3	Eliki	22 ¹ 25–30 ³ 13– 15 ¹⁰	12.5 ¹	6.7 ⁵	1.56 ¹ 0.35–1.2 ² 1.0 ¹¹	6 ¹ 3–8 ³ 4–10 ⁹	373 BC ¹² 1402 AD ¹² December 26, 1861 ¹² /6.6 ² 6.7 ^{1,4} July 6, 1965/ 6.3 ^{1,13}	260 ¹ 242±60 ⁹
4	Offshore Akrata	8 ¹	8 ¹	5.7 ¹	0.19 ¹	5 ¹ 3–5 ¹⁴	November 18, 1992/ 5.7 ^{1,15}	40 ¹
5	Xylokastro	20 ¹ 25–30 ³	17 ¹	6.7 ⁴	1.26 ¹	5 ¹ 6–7 ³ 5 ³ 6 ⁹	February 21, 1742/ 6.7 ^{1,5} March 6, 1753/ 6.1 ^{1,5} April 8, 1970/ 6.2 ^{1,16}	252 ¹ 138±20 ⁹
6	Offshore Perachora	18 ¹ 11.2 ¹⁷	16 ¹	6.5 ⁵	0.54 ¹	4 ¹	April 16, 1775/ 6.0 ^{1,4, 5} October 3, 1887/6.5 ^{1,4, 5} April 22, 1928 6.3 ^{1,4, 5}	135 ¹
7	Skinos	19 ¹ 15–20 ³	19 ¹ 14 ¹⁸	6.7	0.96 ¹ 1.4 ¹⁹ 1.3 ¹⁸	3 ¹ 2 ¹⁵	February 24, 1981/6.7 ^{1,20}	319 ¹ 330 ¹⁹
8	Alepochori	13 ¹ 15–20 ³	13 ¹ 13 ¹⁸	6.4	0.71 ¹ 0.66 ¹⁸ 1.0 ²⁰	3 ¹ 1.8 ³	February 25, 1981/ 6.4 ^{1,21}	285 ¹

^aReferences are as follows: (1) this study, (2) Bernard et al. [2006], (3) Armijo et al. [1996], (4) Ambraseys and Jackson [1997], (5) Papazachos and Papazachou [2003], (6) Pantosti et al. [2004], (7) Bernard et al. [1997], (8) Galanopoulos [1953], (9) Briole et al. [2000], (10) Marinatos [1960], (11) Schmidt [1879], (12) Mouyaris et al. [1992], (13) Baker et al. [1997], (14) Bell et al. [2009], (15) Hatzfeld et al. [1996], (16) Liotier [1989], (17) Stefatos et al. [2002], (18) Hubert et al. [1996], (19) Collier et al. [1998], (20) Jackson et al. [1982], and (21) Taymaz et al. [1991].

neighboring segments has a static triggering effect, that is, if a specific segment is moved closer to or farther away from failure by the static stress change caused by the coseismic slip at the time of occurrence of such earthquakes. For this purpose, the methodology adopted by Console et al. [2008, 2010] and Parsons et al. [2012] is followed, in which the Coulomb stress transfer is computed on the target fault segments, by resolving on their specific focal mechanism the tensorial coseismic stress changes associated with the major earthquakes in the area. Previous geological studies, recently collected accurate seismological data and geodetic measurements, as well as the geomorphological features of the area, were used to define the faults, which were considered as single dislocation planes in an elastic, homogeneous half-space. The present state of stress can help to identify areas of high potential for the occurrence in the Corinth Gulf of moderate-to-strong earthquakes in the next 30 years.

2. Fault Segmentation and Definition of the Seismic Sources

[9] It is now widely accepted for our study area that the subcrustal lithosphere and lower crust deform in a ductile manner, and that seismically active faults affect only the upper brittle crust [e.g., Jackson and White, 1989; Hatzfeld et al., 2000], which is being continuously loaded at a certain long-term slip rate. A sudden change in stress, however, may alter the probability of occurrence of the next strong event on a particular fault or fault segment. For the purpose of the present study, a seismic source model is adopted and used as an input for the calculation of probabilities, based on certain segmentation criteria and information on historical

and instrumental seismicity. The stick-slip regions are close and thus are expected to interact through stress coupling because they do not come fully to the surface. Near to the surface, and near to the upper bound and the base of the seismogenic layer, stick-slip events contribute only a moderate amount of slip [King et al., 1994a]. It seems that complete stress coupling and stick-slip behavior can only occur in a narrow region at the center of a seismogenic zone.

[10] Since $M_w \sim 6$ events in this area completely cut the seismogenic zone, our sources are assumed to behave in this way. On the other hand, their interaction is expected to be significant, because their L/W ratios are small as indicated by Lin and Stein [2004].

[11] In Figure 4, the major fault segments of the Corinth Gulf and macroseismic epicenters of historical events ($M_w > 6.0$) that occurred after 1700 AD are shown. All the epicenters of historical earthquakes in this figure have been plotted as they are published in the catalog of Papazachos and Papazachou [2003]. These sites imply the macroseismic rather than the microseismic epicenters, but we preferred not to make any changes for plotting purposes. However, each one of the earthquakes has been attributed to each one of the major faults in Table 1, taking into account not only their epicenters but also all the available macroseismic information [Papazachos and Papazachou, 2003; Ambraseys, 2009]. For this reason, some of the earthquakes in the map are missing in Table 1, such as the earthquakes of 1703, 1756, and 1769 in the westernmost part of the gulf. The 1703 earthquake caused very limited damage to a part of the castle in Nafpaktos, an old and probably not in good condition building [Ambraseys, 2009]. Thus, its magnitude is probably lower than 6.0, and it was most likely associated

Table 2. Geometric Parameters Considered in This Paper for the Eight Fault Segments, Along the Southern Bound of Corinth Gulf

Segment Number	Segment Name	Strike (°) ±10°	Dip (°) ±5°	Rake (°) ±10°	Length (km) ±5 km	Width (km) ±2 km	Depth of the Fault Center (km) ±0.5
1	Psathopyrgos	270	45	270	15	10	7.5
2	Aigion	277	33	284	16	10	7.5
3	Eliki	281	34	289	22	12.5	7.5
4	Offshore Akrata	270	30	279	8	8	7.5
5	Xylokaastro	265	23	279	20	17	7.5
6	Offshore Perachora	285	40	290	18	16	7.5
7	Skinos	264	42	280	19	15	- 7.5
8	Alepochori	261	44	275	13	13	7.5

with other secondary faults as suggested in other studies [Bernard et al., 2006; Karakostas et al., 2012]. According to Ambraseys [2009], contemporary reports to the 1756 earthquake confirm that the epicentral area was to the north central part of the gulf of Corinth. Regarding the 1769 earthquake, it caused damage in a broad area from Antirrio to Desfina. However, cumulative evidence of the source material and the seismicity of the region support a link with the Desfina earthquake [Ambraseys, 2009].

[12] The seismically active faults are mainly the north-dipping faults that bound the Gulf to the south (Figure 4). Seismicity is associated with the *Psathopyrgos*, *Aigion*, *Eliki*, and *Xylokaastro* faults in the western and central parts of the Gulf. These fault segments have an average strike of 270°–285° and a northward dip of about 50° near the surface.

[13] The eastern extremity of the Gulf of Corinth is more complex, with the main active normal fault segments, *Offshore Perachora*, *Skinos*, and *Alepochori*, striking more north-eastward (250°–270°) and cutting obliquely across both structures and the relief. Nevertheless, there is clearly no major seismicity related to the steep south-dipping faults that bound the Gulf of Corinth to the north, which may be interpreted as antithetic faults. Most of the well-determined mechanisms indicate nodal planes dipping 30°–40° to north and steeper south-dipping planes [see, e.g., Baker et al., 1997], evidencing the asymmetry of the Corinth rift.

[14] In view of this observation, and having regard to the available tectonic and seismological studies, we consider that strain released by strong main shocks along the Gulf is mostly accumulated on eight major fault segments, if we include to the above the *Offshore Akrata* segment (numbered 4 in Figure 4), striking almost east west and following the shape of the Gulf. Other fault segments are considered as secondary ones and their seismicity is considered to be the result

of stress redistribution caused by the major ruptures. We assume that major segments rupture individually, without excluding the possibility that in future, some of them could break simultaneously with the adjacent ones. Contrarily, there are instances where the aforementioned segments failed partially, as will be revealed later, when dealing with their activation. Table 1 lists these fault segments and gives information on their linear dimensions, average slip per event, slip rate, and recurrence time. Fault lengths were assigned based on reported information as shown in the reference list of Table 1, together with evaluations performed in the present study in connection with values derived from proper scaling laws [Wells and Coppersmith, 1994; Papazachos et al., 2004]. The final values adopted in our study are in full agreement with the statement that the dimensions along the strike of normal faults do not exceed 20–25 km [Jackson and White, 1989], which implies an upper limit for the magnitude of the earthquakes that can occur on individual fault segments.

[15] The fault width was directly calculated from the width of the seismogenic layer considering the dip angle of each segment. The effective seismogenic layer is 10–12 km outside the Gulf and only 7–8 km beneath the Gulf [Briole et al., 2000]. Local seismicity data indicate that the seismogenic layer is in the depth range 5–13 km, varying between fault segments [Rigo et al., 1996; Hatzfeld et al., 2000]. In our source models, we selected different values for the width of the activated fault segments, observing the constraint that the width of a fault segment should not exceed its length (see Table 1). It is worthy to mention here that the available information from previous investigations is taken into account, which along with calculations of source parameters from scaling laws, slight simplifications for defining planar rectangular fault surfaces, and compromising diversity

Table 3. Parameters Considered in This Paper for the Computation of the Clock Change and Conditioned Probability Related to the Eight Fault Segments

Segment Number	Segment Name	Coseismic Slip (m) ±30%	Slip rate (mm/yr) ±30%	Tectonic Stressing Average Rate (kPa/yr)	Recurrence Time (yr) ±60%	Alpha ±0.45
1	Psathopyrgos	0.75	6	61 ±32	125	0.55
2	Aigion	0.88	6	59 ±30	147	0.55
3	Eliki	1.56	6	43 ±20	260	0.55
4	Offshore Akrata	0.19	Not considered		Not considered	Not considered
5	Xylokaastro	1.26	5	32 ±15	252	0.55
6	Offshore Perachora	0.54	4	28 ±13	135	0.55
7	Skinos	0.96	Not considered		Not considered	Not considered
8	Alepochori	0.71	Not considered		Not considered	Not considered

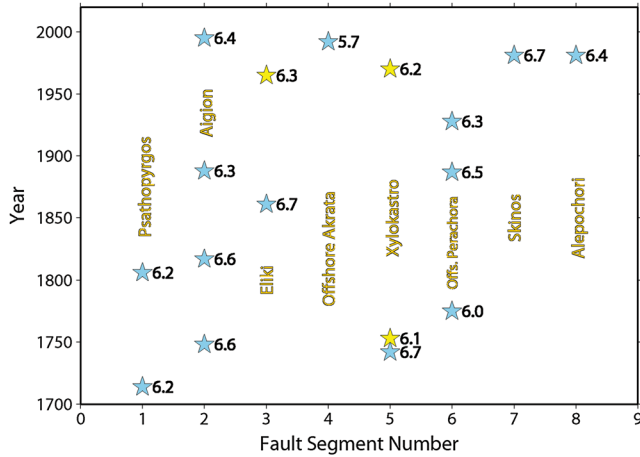


Figure 5. Temporal distribution of the characteristic earthquakes along the eight fault segments adopted for modeling the seismogenic structure following the southern bound of the Corinth rift. Yellow stars indicate the three events with significantly smaller magnitudes than the magnitudes of the characteristic events that broke entirely the segments 3 and 5.

in the different opinions, the parameter values listed in Tables 2 and 3 are the ones adopted for our calculations. The dimensions of the aftershock zones of recent strong earthquakes, the seismically released strain as well as the seismic moment of the characteristic earthquake in each fault segment were used for the calculation of the mean return periods (column sixth in Table 3). These values have been obtained by dividing the coseismic slip (column third in Table 3) by the tectonic loading (long-term slip rate, column fourth in Table 3). The slip rates assigned to each fault segment are based on published geodetic data.

[16] The values of coseismic average slip were computed by the formula [Console *et al.*, 2008, equation A3]:

$$\bar{\Delta u} = \frac{\pi^2 \Delta \sigma}{32 \mu} (WL)^{1/2} \quad (1)$$

where L and W (sixth and seventh columns in Table 2, respectively) are the length and width of a fault with rectangular shape, μ is the shear modulus of the elastic medium ($3.3 \cdot 10^{10}$ Pa) [Scholz, 2002], and $\Delta \sigma$ is the stress drop ($3 \cdot 10^6$ Pa) [Console and Catalli, 2006].

[17] The mean return periods, in general, are in agreement with those previously determined in the references given next to each value in Table 1. The following formula is used for converting magnitude into seismic moment [Papazachos *et al.*, 1997]:

$$\log M_0 = 1.5 M_w + 15.99 \quad (2)$$

[18] The deformation is localized in a narrow deforming zone, in particular, in the western part of the rift where strain rates reach values of $4.5 \times 10^{-14} \text{ s}^{-1}$ [Briole *et al.*, 2000]. The north-south extensional strain across the Corinth rift has occurred at an average 10–12 mm/yr since about 1890 [Billiris *et al.*, 1991; Davies *et al.*, 1997]. Clarke *et al.* [1997] resolve a slip rate of 11–13 mm/yr across the western Gulf of Corinth, decreasing toward the eastern end. These

authors obtained a slip rate of approximately 3 mm/yr at the longitude of the Alkyonides Gulf basin-bounding faults. Thus, slip rates are largest in the western segments and decrease toward the eastern end of the Gulf (Table 1). They are assigned to each fault segment, based as mentioned above, on published geodetic data, assuming that the seismic part of this motion is 60% of the total slip, with the choice of seismic coupling coefficient being based on previous relevant investigations. According to Ambraseys and Jackson [1990], a significant proportion (as much as 60%) of the strain may be aseismic. Jackson *et al.* [1994] made estimates of regional medium-term seismic hazard based on the difference between geodetic deformation and that predicted from the seismic release of strain and concluded that seismicity can account for at most 50% of the deformation in the Aegean area. Davies *et al.* [1997] found that the seismic expression of strain for Greece, calculated from the seismic moment tensors of earthquakes of $M_w \geq 5.8$, accounts for only 20–50% of the geodetically determined strain. The above are in accordance with relevant investigations in other regions, for example. King *et al.* [1994a] compared plate rates to seismic moment release rates, assuming a typical seismogenic layer thickness of 15 km (below a locking depth deformation is continuous without earthquakes, while above that depth, the faulting is seismic and the motion can therefore be modeled by vertical dislocations positioned beneath the mean location of the surface faulting) in the area of California and Nevada. They found that the relative plate motion occurred about 60% seismically and 40% aseismically.

[19] The major fault segments that bound the Corinth Gulf to the south are considered both as causative faults and receivers in our stress calculation model. In addition to these, the neighboring ones activated during the last five decades are included in the group of causative faults. Two of these segments are also north-dipping normal faults, associated with the 6 July 1965 $M_w 6.3$ and 8 April 1970 $M_w 6.2$ events occurred on East part of Eliki and East of Xylokaastro faults, respectively. Considering that recent events adjacent to our fault zone may exert stress changes that will influence probability calculations, the Trichonida fault segment associated with the 1975 ($M_w 6.0$) event, the Kapareli fault segment associated with the third 1981 main shock ($M_w 6.3$), and the fault segment associated with the Achaia 2008 ($M 6.4$) earthquake are also incorporated (Figure 4).

[20] Historical information and instrumental data give the association between fault segments and events reported in Table 1. This association is also shown graphically in the space-time plot of Figure 5. Note that in Figure 5, events of 6 March 1753 ($M_w 6.1$), 6 July 1965 ($M_w 6.3$), and 8 April 1970 ($M_w 6.2$) of Table 1 are represented by yellow stars and other events by blue stars. The reason for this is that these three events had significantly smaller magnitudes than the magnitudes of the characteristic earthquakes that broke the entire segments 3 and 5 of Table 1. 6 March 1753 earthquake ($M_w 6.1$) may be regarded in a broad sense as an aftershock of 21 February 1742 event ($M_w 6.7$), and we associate it to the main shock in our analysis. Strong events seem rather random and quite evenly distributed among the main fault segments, which have exhibited repeating activation in the last three centuries. One may, however, postulate a migration from east to west, and in particular that activity started at the

western part when an event had already occurred in the eastern part of the study area. Being more specific, during 1714–1775, the *Psathopyrgos*, *Aigion*, *Xylokaastro*, and *Offshore Perachora* segments ruptured (see Figure 4). Activity shifted to the west soon after in 1806, to the *Psathopyrgos* fault, and then continued during 1806–1887 again up to the *Offshore Perachora*. The next two comparatively moderate events in *Aigion* and *Offshore Perachora*, both of M_w 6.3, formed a smaller group, with the last one being between 1965 (*East Eliki* fault) and 1981 (*Alepochori*). After the seismic sequences in the easternmost part of the Gulf in 1981, strong events are concentrated in the central and western parts of the Gulf. This seems in agreement with *Scholz* [2010] who presented evidence that synchronization is occurring between fault segments moving at similar slip rates. Even though historical data are incomplete, the author has shown that there is no exact repetition of individual ruptures or clusters of ruptures, as in our study, and this was attributed to the complexity of fault systems, although the signature of synchronicity is found to be clearly evident. Stress transfer among neighboring fault systems is a possible driving mechanism for such migration patterns. However, other mechanisms of external loading that could synchronize earthquakes on a set of faults have been proposed, such as fluid or magma intrusion, or aseismic transients such as slow earthquakes [*Marsan et al.*, 2013]

3. Conditional Probability Computed Under Renewal Models

3.1. Renewal Models

[21] Especially since the 1970s [e.g., *Vere-Jones*, 1970, 1978; *Utsu*, 1972], earthquake recurrence is frequently considered as a renewal process rather than one with no memory of the preceding large shock. In a renewal process, the times between successive events, in this case the large earthquakes in a fault are assumed to be independent and identically distributed random variables. In this interpretation, the expected time of the next event only depends on the time of the last event. In combination with the elastic rebound theory, the probability of another earthquake would be low just after a fault-rupturing earthquake and would then gradually increase, as tectonic deformation slowly stresses the fault again. When an earthquake finally occurs, it resets the renewal process to its initial state. Several popular statistical models (such as the log-normal, gamma, BPT, and Weibull distributions) have been often used to describe the quasi-periodic occurrence of large earthquakes and estimate future earthquake conditional probabilities for particular faults [*Mosca et al.*, 2012]. They share several properties that are commonly observed for earthquake interevent times. These distributions may fit the empirical data well even if there is no physical justification for their use. *Mosca et al.* [2012], analyzing well-documented paleoseismological and historical sequences, conclude that the BPT model performs better than the other models (log-normal, double exponential, and gamma) except for Weibull. For this reason, and considering that the BPT model has gained wide acceptance in the last decade, we limited our attention in the analysis of the Corinth Gulf seismic sequences to the BPT and the Weibull models only.

[22] A characteristic of the BPT distribution is that when the conditional probabilities of event occurrence are calculated for windows well after the mean recurrence time, they approach a constant asymptote. This characteristic is shared by a discrete-time box-filling model presented by *Gonzalez et al.* [2006]. In contrast, the log-normal distribution predicts that the conditional probability of event occurrence slowly declines with increasing time after passing through a maximum. For the Weibull and gamma distributions, the conditional probability can be increasing or decreasing as the elapsed time from the last event tends to infinity, depending on the parameters of these distributions. There is a modification of the BPT model that includes the viscoelastic response of the lower crust and upper mantle to large earthquakes or deep post seismic slip [e.g., *Michael*, 2005]. Both of these processes result in a temporarily higher rate of loading on the seismogenic fault for some time after a large event. In this way, the loading of strain energy onto seismogenic faults is not temporally uniform as in the BPT and Weibull models. This inclusion in the BPT model may not improve the ability to make empirical fits to observed earthquake recurrence data because both transient deformation and uniform loading curves can yield similar interevent time distributions if all parameters are used solely to fit recurrence data.

[23] In this paper, we only use the simple BPT and Weibull models, even though we are aware that including the viscoelastic response in the BPT model might be more realistic and could have an impact on the effect of the static stress changes. Evaluation of how the viscoelastic response might affect forecast performance of earthquakes renewal models is left to future studies.

3.2. The BPT and Weibull Distributions

[24] In an extremely simplified approach, only earthquakes that break all or most of the area of a fault segment are considered in the computation of total seismic moment release, and as the characteristic earthquakes of the specific segment. Statistically, their occurrence is represented as a point process, and the interevent time is modeled by a probability density function (*pdf*). In this context, the null hypothesis is that the earthquake process has no memory (described by a uniform Poisson model). For a uniform Poisson model, the earthquake hazard is constant in time, and the *pdf* is a negative exponential function:

$$f(t) = \frac{1}{T_r} \exp\left\{-\frac{t}{T_r}\right\} \quad (3)$$

where t is the time elapsed since the latest characteristic earthquake, and T_r is the mean interevent time, i.e., the average recurrence time. In the Poisson model, only one parameter, the interevent time, is necessary for a complete description. On the other hand, the characteristic earthquake hypothesis needs a more elaborate model, called a renewal model, whose *pdf* contains one more free parameter, conditioning the shape of the distribution in terms of its periodicity [*Shimazaki and Nakata*, 1980]. The *pdf* of interevent times for a renewal model has a mode close to its expected recurrence time. Consequently, the earthquake hazard is small immediately following the previous characteristic earthquake and then initially increases as time elapses without a further event occurring [*McCann et al.*, 1979].

Table 4. Characteristic Earthquakes Reported for the Southern Corinth Gulf Fault System

Event Number	Year	Month	Date	M	Fault Name	Segment Number
1.	1714	7	29	6.2	Psathopyrgos	1
2.	1742	2	21	6.7	Xylokaastro	5
3.	1748	5	25	6.6	Aigion	2
4.	1753	3	6	6.1	Xylokaastro	5
5.	1775	4	16	6.0	Offshore Perachora	6
6.	1806	1	24	6.2	Psathopyrgos	1
7.	1817	8	23	6.6	Aigion	2
8.	1861	12	26	6.7	Eliki	3
9.	1887	10	3	6.5	Offshore Perachora	6
10.	1888	9	9	6.3	Aigion	2
11.	1928	4	22	6.3	Offshore Perachora	6
12.	1965	7	6	6.3	Eliki	3
13.	1970	4	8	6.2	Xylokaastro	5
14.	1981	2	24	6.7	Skinos	7
15.	1981	2	25	6.4	Aleporochori	8
16.	1992	11	18	5.7	Offshore Akrata	4
17.	1995	6	15	6.4	Aigion	2

[25] Under the plain characteristic earthquake hypothesis, the fault segments are supposed to behave independently from each other according to the probability distribution of the interevent times.

[26] The BPT *pdf* [Matthews *et al.*, 2002] is given by:

$$f(t, T_r, \alpha) = \left(\frac{T_r}{2\pi\alpha^2 t^3}\right)^{1/2} \exp\left\{-\frac{(t - T_r)^2}{2T_r\alpha^2 t}\right\} \quad (4)$$

where α is the coefficient of variation (also known as the aperiodicity) of the distribution. The coefficient of variation is the standard deviation of interevent times between large events that rupture all or most of a given fault segment divided by the mean repeat time for that segment. It is a key parameter in time-varying probability calculations.

[27] An alternative interevent time distribution tested in this study is the Weibull distribution [Weibull, 1951]:

$$f(t, T_r, \gamma) = \frac{\gamma}{T_r} \left(\frac{t}{T_r}\right)^{\gamma-1} \exp\left\{-\left(\frac{t}{T_r}\right)^\gamma\right\} \quad (5)$$

where γ is the shape parameter of the distribution, defined as the inverse of the coefficient of variation.

[28] The probability for the occurrence of a new event in a given time window Δt , conditional on no events occurring before time t , is obtained from the density distribution of the interevent times:

$$Pr[t < T \leq t + \Delta t | T > t] = \frac{Pr[t < T \leq t + \Delta t]}{Pr[t < T]} = \frac{\int_t^{t+\Delta t} f(u) du}{1 - \int_0^t f(u) du} \quad (6)$$

[29] Given appropriate values for α and γ , the *pdf* for the BPT and Weibull models may appear rather similar, but the hazard functions (the instantaneous values of the conditional rate density) may be quite different. Typically, while the hazard function for the BPT distribution starts from zero soon after an event, it increases as the elapsed time approaches the recurrence time, and then asymptotes to a stable value, the hazard function for the Weibull distribution keeps increasing indefinitely as the elapsed time exceeds the recurrence time. These comments on the hazard function apply only if the coefficient of variation is smaller than unity, as observed in

many, but not all, sequences of large earthquakes in specific faults.

3.3. Application to Our Data Set

[30] In our application to the seismic sources of the Corinth Gulf area, we have adopted the recurrence times listed in Table 3. Such values come from the ratio between the total slip (i.e., coseismic slip, $\overline{\Delta u}$) and slip rate, $\Delta \dot{u}$, third and fourth columns in Table 3, respectively. We consider that the uncertainties in the coseismic slip and slip rate can exceed 30% of the assigned values. Consequently, if the errors in these parameters are absolute errors, we estimate the uncertainty of the recurrence periods in this way:

$$\Delta T_r = (\Delta(\overline{\Delta u})/\overline{\Delta u} + \Delta(\Delta \dot{u})/\Delta \dot{u}) * T_r \quad (7)$$

[31] For the variability of the coefficient of variation, Sykes and Menke [2006] examined segments of very active faults along plate boundaries of the transform and subduction type in Japan, Alaska, California, Cascadia, and Turkey, considering values of α from 0 to 0.5 ± 0.2 . They highlighted the bias that a much larger or smaller value of α can have on the estimate of future ruptures. Their considerations were based on a Bayesian technique to suppress measurement uncertainties in the dates of paleoseismic earthquakes and to derive intrinsic estimates of repeat time and its normalized standard deviation (i.e., coefficient of variation), and their uncertainties. For example, a much larger value of α assigned at a few faults can lead to an advance in their cycle of stress buildup to their next large earthquakes and a too low probability of rupture in the next few decades. While for an α of about 0.2, mean repeat time needs to be shorter than about 150 years for forecasts generally to be useful on timescales of a few decades. Scharer *et al.* [2010] considered a coefficient of variation slightly higher than previous estimates, of ~ 0.7 , for quasi-periodic recurrence of large earthquakes on the southern San Andreas Fault (California). In this study, keeping in consideration the above mentioned papers, in the absence of any statistical assessment, due to the very low number of events reported on each segment (Table 4), we have considered for α its maximum variability, as we are aware that it is a key parameter in time-varying

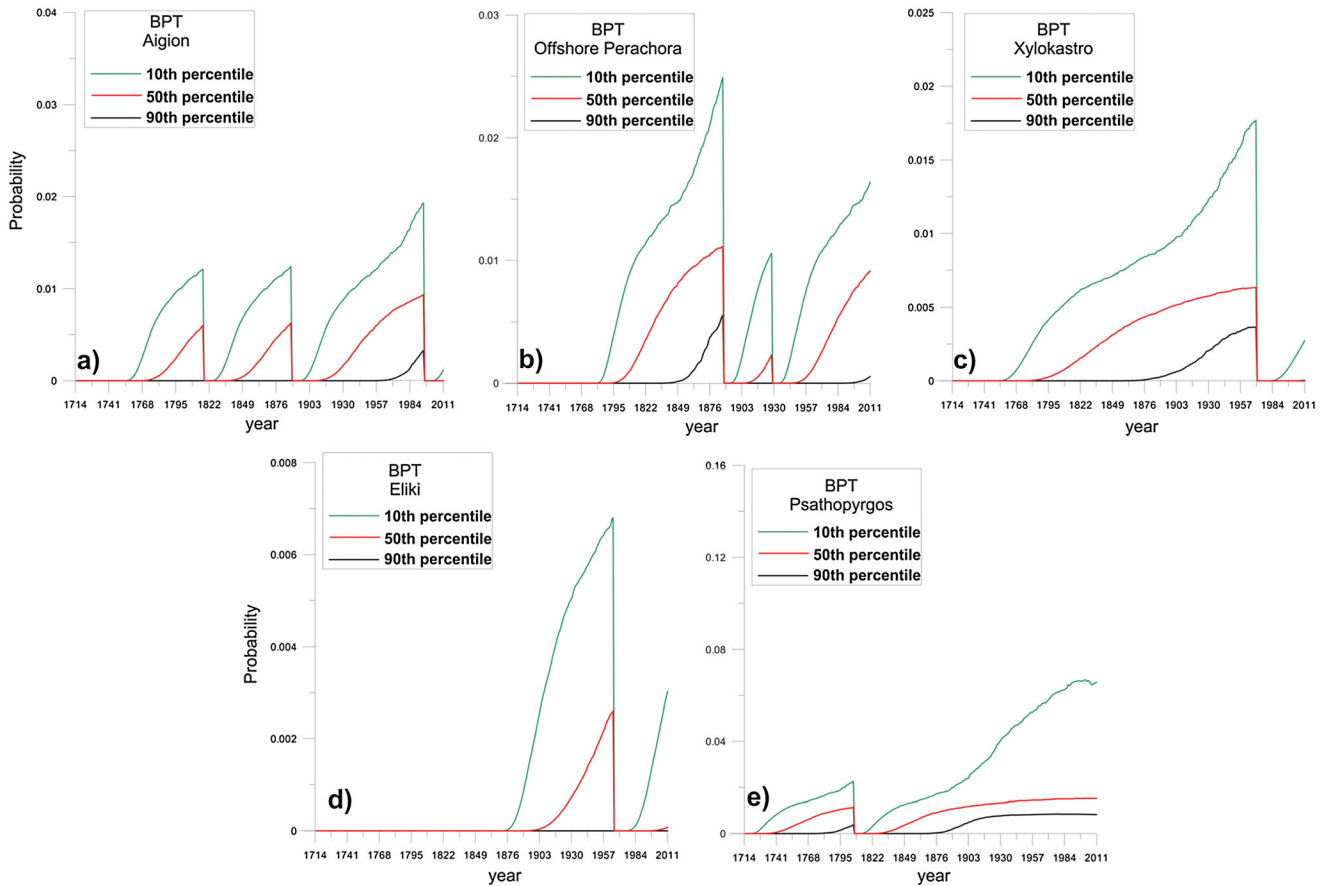


Figure 6. Conditional probability of occurrence of a characteristic earthquake computed under the BPT model for five of the eight fault segments adopted for modeling the seismogenic structure following the southern bound of the Corinth rift. (a) Aigion. (b) Offshore Perachora. (c) Xylokaastro. (d) Eliki. (e) Psathopyrgos. The plots show the results of a Monte Carlo procedure applied to the uncertainties in the parameters of the interevent time distribution.

probability estimates. Consequently we have adopted a value of $\alpha = 0.55$ with an uncertainty of ± 0.45 .

[32] By means of equation (6), we have computed the probability of occurrence for a characteristic earthquake on each of the eight fault segments listed in Table 1, in steps of 1 year after 1700 AD. The computation starts at the time of occurrence of the first characteristic earthquake on each segment listed with apex 1 in the eighth column of Table 1, and the elapsed time is reset to zero upon the occurrence of every subsequent event.

[33] The computations are repeated 1000 times in a Monte Carlo procedure by randomly drawing both the interevent time and the coefficient of variation from a uniform distribution within their respective uncertainties (Table 3). Among the 1000 outcomes, we have considered the tenth, fiftieth, and ninetieth percentiles. The results are shown in Figures 6 and 7, for the BPT and the Weibull distributions, respectively, limiting our analysis to segments 1 (*Psathopyrgos*), 2 (*Aigion*), 3 (*Eliki*), 5 (*Xylokaastro*), and 6 (*Offshore Perachora*). These are the segments for which at least two events after 1700 AD are reported.

4. Effect of the Stress Transfer

[34] Earthquakes are considered to interact with one another. In fact, according to the theory of elasticity, the

coseismic slip of an earthquake associated with a certain fault segment results in a redistribution of the stress in the surrounding crustal volume. The Coulomb Failure Function (*CFF*) is a linear combination of the changes in the shear and normal stress on the fault plane of a particular earthquake source. Its coseismic static stress change is then given by [King *et al.*, 1994b; King and Cocco, 2001]:

$$\Delta CFF = \Delta\tau + \mu' \cdot \Delta\sigma_n \quad (8)$$

where $\Delta\tau$ is the shear stress change on the receiving fault (computed in the slip direction) and $\Delta\sigma_n$ is the normal stress change acting on the receiver fault (positive for unclamping or extension).

[35] $\mu' = \mu(1-B)$ is usually called the effective friction coefficient (μ is the friction coefficient), and B is the Skempton coefficient which varies between 0 and 1 [Beeler *et al.*, 2000; Cocco and Rice, 2002]. A span of effective friction coefficient between 0 and 0.8 is considered here, which is making a common assumption that pore fluid response to static stress change is encompassed [Parsons, 2005]. The 0.8 value is appropriate for aftershock sequences, meaning just after the main rupture when the water is “escaped” from the fault. When we are far (in time) from the rupture, as in our cases, it should not be greater (this means no computations

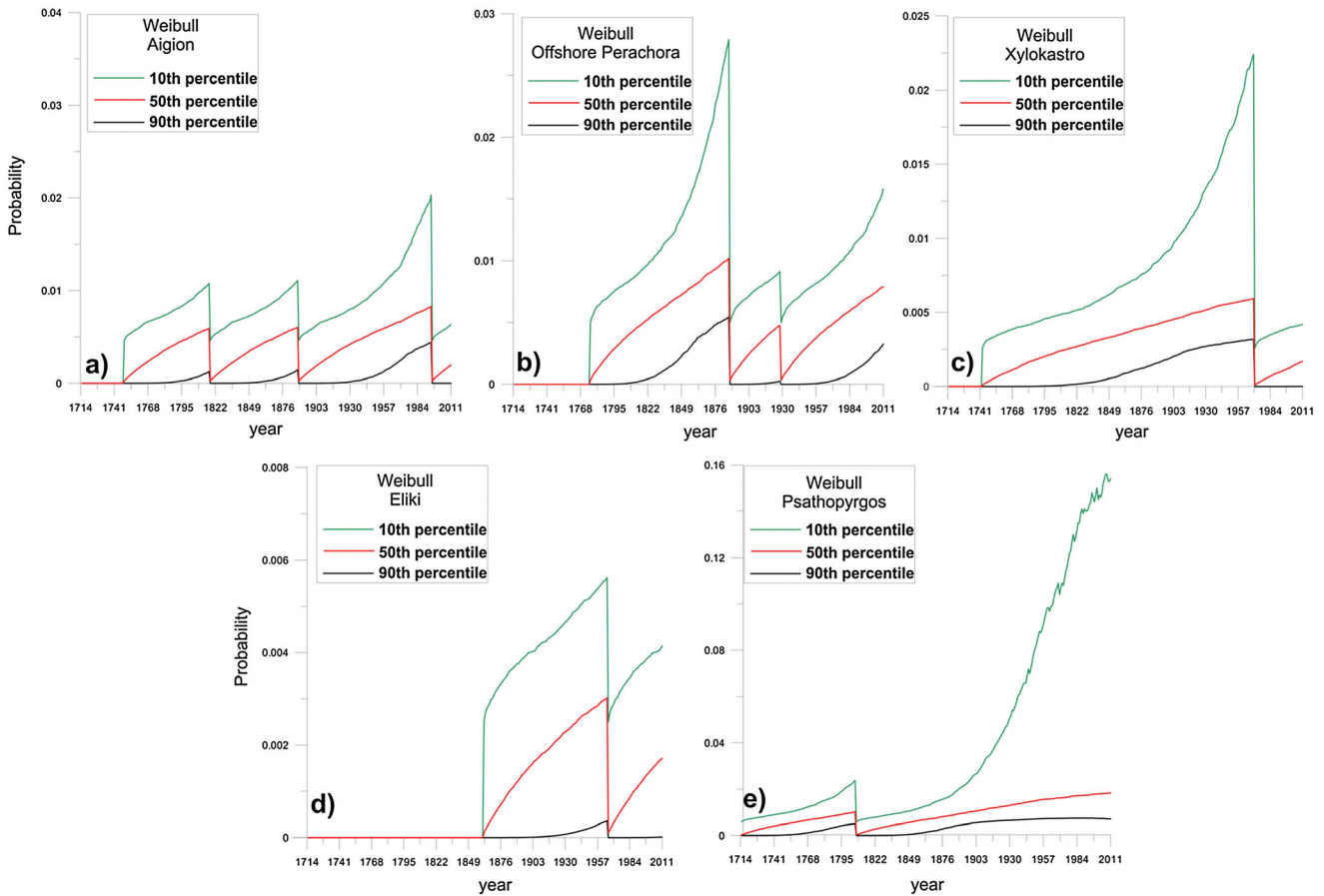


Figure 7. Conditional probability for the occurrence of a characteristic earthquake computed under the Weibull model for five of the eight fault segments considered for modeling the seismogenic structure following the southern bound of the Corinth rift. (a) Aigion. (b) Offshore Perachora. (c) Xylokaastro. (d) Eliki. (e) Psathopyrgos. The plots show the results of a Monte Carlo procedure applied to the uncertainties in the parameters of the interevent time distribution.

for $\mu' = 0.9$). The values lower than 0.3 are entertained to satisfy weak fault models that have been suggested for Corinth Gulf major faults [Chery, 2001]. This assumption could well be incorrect [Beeler et al., 2000], since it is not known how fault fluids are distributed, or how they respond to static stress change. According to several authors [Harris, 1998; King and Cocco, 2001; Catalli et al., 2008], anyway, the effect of the friction coefficient on the stress perturbation and the seismicity rate change patterns is usually unremarkably modest.

[36] It is clear that the computation of ΔCFF requires knowledge of the mechanism of both the causative and the receiving sources, as well as the slip distribution on the causative sources. In the absence of direct information about the slip distribution for the causative earthquakes considered in this study, we have assumed for all of them a distribution consistent with a uniform stress drop on the rectangle of the segment fault [Console and Catalli, 2006].

[37] In our application to the Corinth Gulf area, we have considered, among the causative sources, not only the eight segments listed in Table 1 (shown in red in Figure 4) but also some sources located in the surrounding area (shown in gray in Figure 4). Horizontal projections of the dislocation planes are better viewed in Figure 8, where the sources of 6 July 1965 ($M_w 6.3$) and 8 April 1970 ($M_w 6.2$) (East part of *Eliki* and East part of *Xylokaastro*, respectively) of Table 4 are

depicted by smaller rectangles (white color) with respect to the sources of 26 December 1861 ($M_w 6.7$) and 21 February 1742 ($M_w 6.7$), which broke the entire respective segments 3 and 5 of Table 1 (larger yellow rectangles). In a preliminary analysis, we have noted that the three faults, Trichonida, Kapareli, and Achaia, edging the Corinth Gulf, do not contribute to the static Coulomb stress change of five receiving faults. For this reason, in the Coulomb stress computation, we have only considered the faults in Table 4.

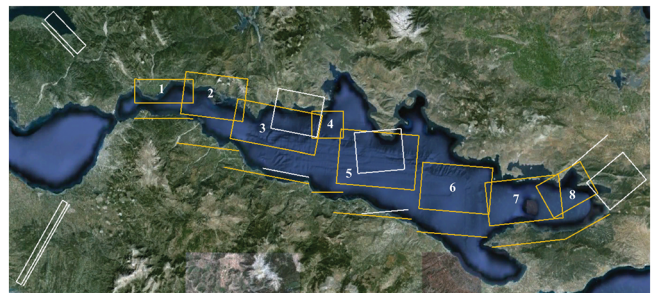


Figure 8. Source modeling in the Corinth Gulf. The eight sources listed in Table 1 are drawn in yellow. Other sources that have been considered for the computation of the Coulomb stress change are drawn in white.

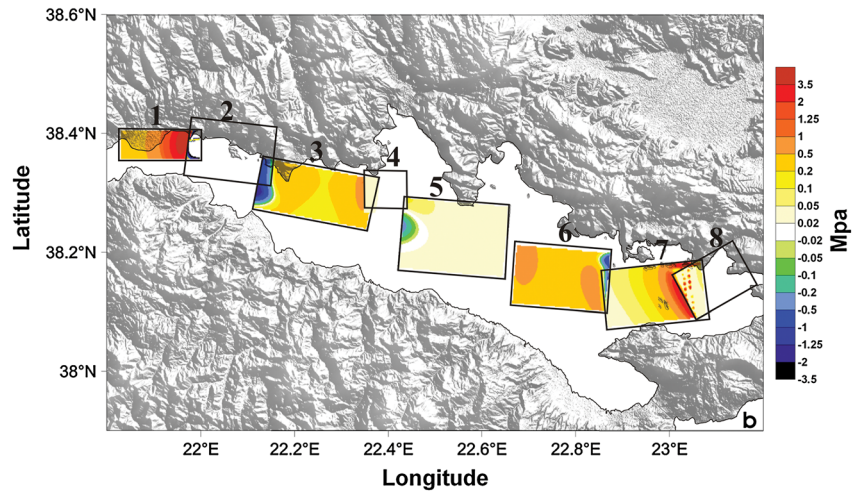


Figure 9. A sample of the Coulomb stress change calculated at the end of the test (December 2011). The eight fault segments are indicated with numbers as in Table 1.

[38] Figure 9 shows a sample of the Monte Carlo procedure for the spatial distribution of ΔCFF obtained by the end of our test (December 2011), mapped on the horizontal projection of the rectangular source segments. Segments 2, 4, and 8 are shown as void spaces, due to the fact that no subsequent events caused significant stress change on these segments after their last characteristic

earthquakes (15 June 1995, 18 November 1992, and 24 February 1981, respectively).

[39] A direct way to incorporate calculated stress changes into earthquake probability calculations is to treat a stress change as an advance or delay in the earthquake cycle. Under the renewal model, fault stress builds with time because of tectonic plate motion. Thus, a sudden stress change

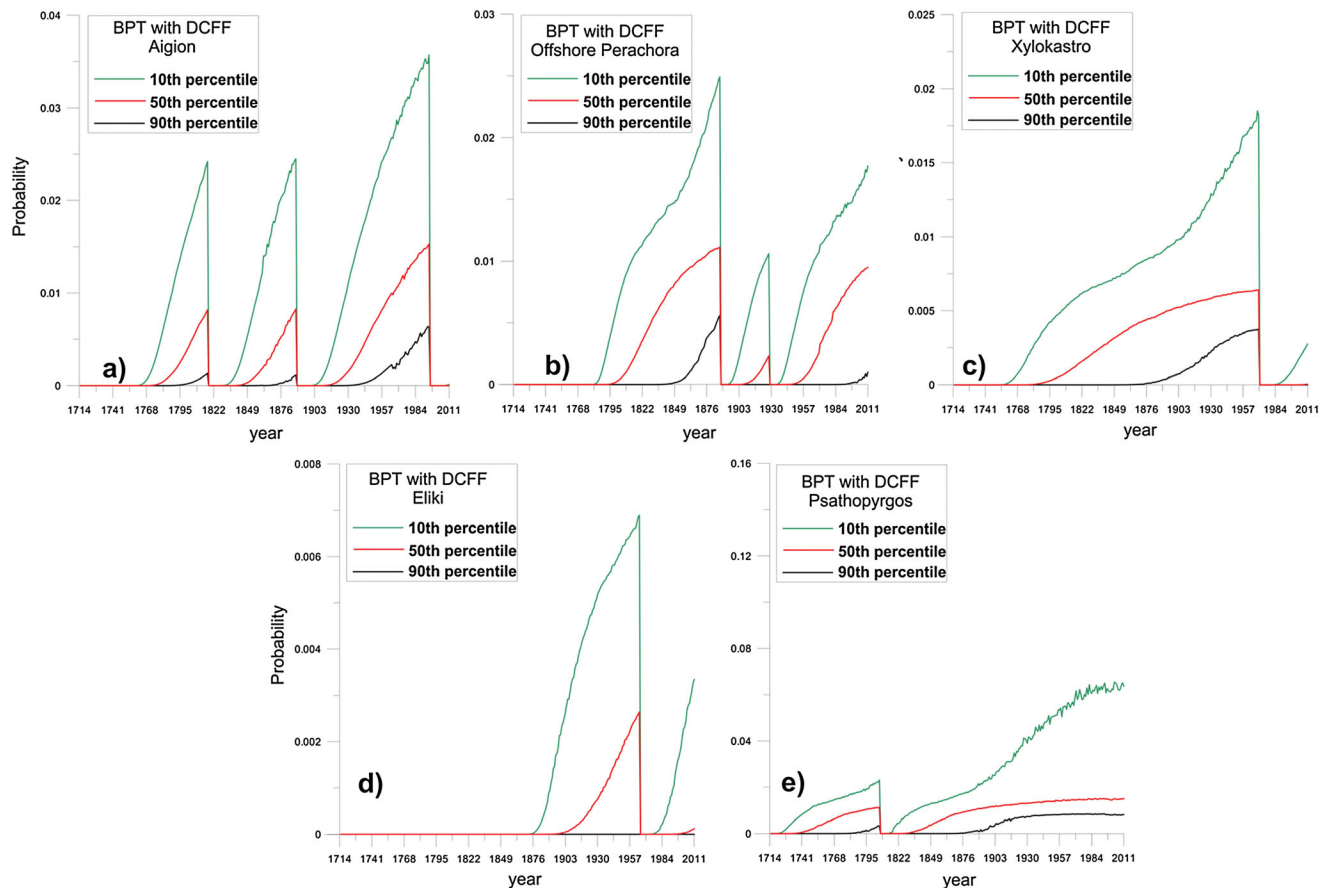


Figure 10. As in Figure 6, with the inclusion of the effect of the stress transfer.

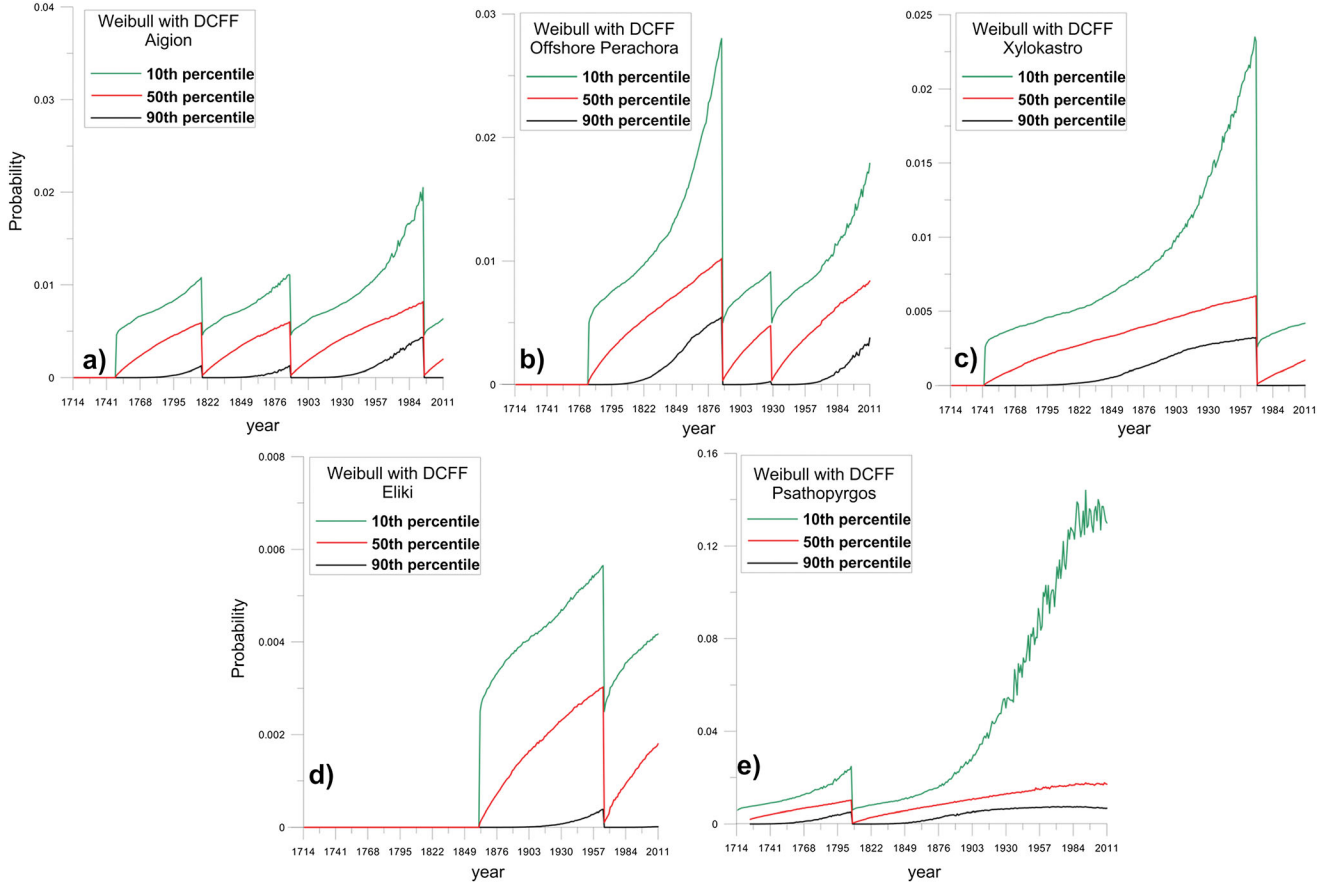


Figure 11. As in Figure 7, with the inclusion of the effect of the stress transfer.

should be equivalent to a sudden shift in the time to the next earthquake that can lead to an advance or delay (clock change, Δt) in the earthquake cycle. This Δt value has a potentially significant effect on the resulting earthquake probability calculation. Thus, we assume that the time elapsed since the previous earthquake is modified from t to t' by a shift, Δt , proportional to ΔCFF [Stein *et al.*, 1997; Parsons, 2005]:

$$t' = t + \Delta t = t + \frac{\Delta CFF}{\dot{\tau}} \quad (9)$$

where $\dot{\tau}$ is the tectonic stressing rate (also named tectonic loading rate), supposed unchanged by the stress perturbation, which in our case can be estimated from the slip rate and the linear dimensions of the earthquake source [see, e.g., Console *et al.*, 2008, equation A9]:

$$\dot{\tau} = \frac{32\mu \cdot \Delta \dot{u}}{\pi^2 \cdot (WL)^{1/2}} \quad (10)$$

[40] In Table 3 for each fault source, we provide the calculated average stressing rates with the respective uncertainties, keeping in consideration the uncertainties related to slip rate and dimensions of the fault.

[41] Since the Coulomb stress change ΔCFF varies over the surface of the target fault segment, ranging typically from negative to positive values, for the application of equation (9), we take a random value drawn from a distribution computed on the nodes of a dense regular grid of 100 cells, with

each side of 10 nodes, reflecting the spatial pattern on the fault, rather than using the average for the whole fault [e.g., Parsons, 2005].

[42] In the computation, the fault dimensions are variable, and accordingly also the spacing is variable, ranging from 1 to 2 km. The spatial coordinates of the grid nodes are computed starting from the coordinates of the fault center, taking into account the width and the dip angle of the fault.

[43] For the fault interaction and for the positive and negative changes in the static Coulomb stress which are shown in Figure 9, we have considered all the eight fault segments adopted for modeling the seismogenic structure following the southern bound of the Corinth rift, whose parameters are reported in Tables 2 and 4.

[44] By the modification of the occurrence time due to clock change, Δt , defined in equation (9), we have recalculated the probability of occurrence in steps of 1 year after 1770 AD, for the BPT and Weibull models, only for the five faults that are associated with more than 1 event, i. e., 1 - Psathopyrgos, 2 - Aigion, 3 - Eliki, 5 - Xylokastro, and 6 - Offshore Perachora, aforementioned as receiving faults, in a similar way as for the unperturbed renewal model adopted in the previous section (Figures 10 and 11). We can see in these figures that the occurrence of earthquakes on some segments produces jumps of the occurrence rate on some of the others, notably on the closest ones. The jumps are always positive, because all the earthquake sources have similar focal mechanisms and they are geographically aligned along the same active structure (along-strike normal faults).

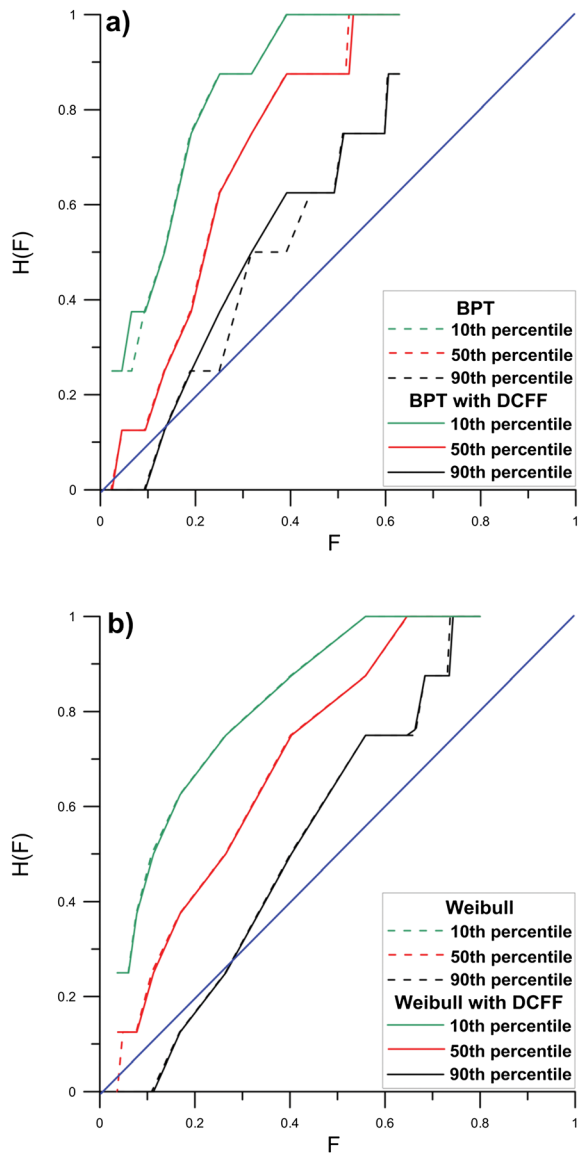


Figure 12. ROC diagram, Hit rate versus the false alarm rate F , for the statistical test of the two renewal models for five fault segments (1, 2, 3, 5, and 6) of the Corinth Gulf. The contribution of the stress change effect (dashed lines) is also considered. (a) ROC diagram for BPT model. (b) ROC diagram for Weibull model. The plots show the results of a Monte Carlo procedure applied to the uncertainties in the parameters of both the interevent distribution and the stress transfer algorithm. The blue line represents the trend of Poisson model.

This circumstance produces a positive ΔCFF and hence a clock advance for the elapsed time. Comparing Figures 10 and 11 with Figures 6 and 7 (probability under the BPT and Weibull models), we can observe that the stress transfer calculations have only a small effect on the results, producing some minor extra wiggles in the probabilities in Figures 10 and 11. And thus it is not surprising that accounting for this phenomena did not improve (or degrade) the results in a significant way.

[45] The other faults, i.e., 4 - Offshore Akkrata, 7 - Skinos, and 8 - Alepochori, having only one historical event (see Table 1) are not considered for the statistical retrospective tests.

[46] In the computation of the stress change and the consequent clock change, we deal with the uncertainties in all the necessary parameters: coefficient of friction, source mechanism parameters, size of the fault, depth of the fault center, coseismic slip, along with the recurrence-time distribution parameters associated to the eight causative and five receiving fault segments considered in this study. The computations are repeated 1000 times in a Monte Carlo procedure by randomly drawing all the above mentioned parameters from a uniform distribution within their respective uncertainties (Table 2 and Table 3).

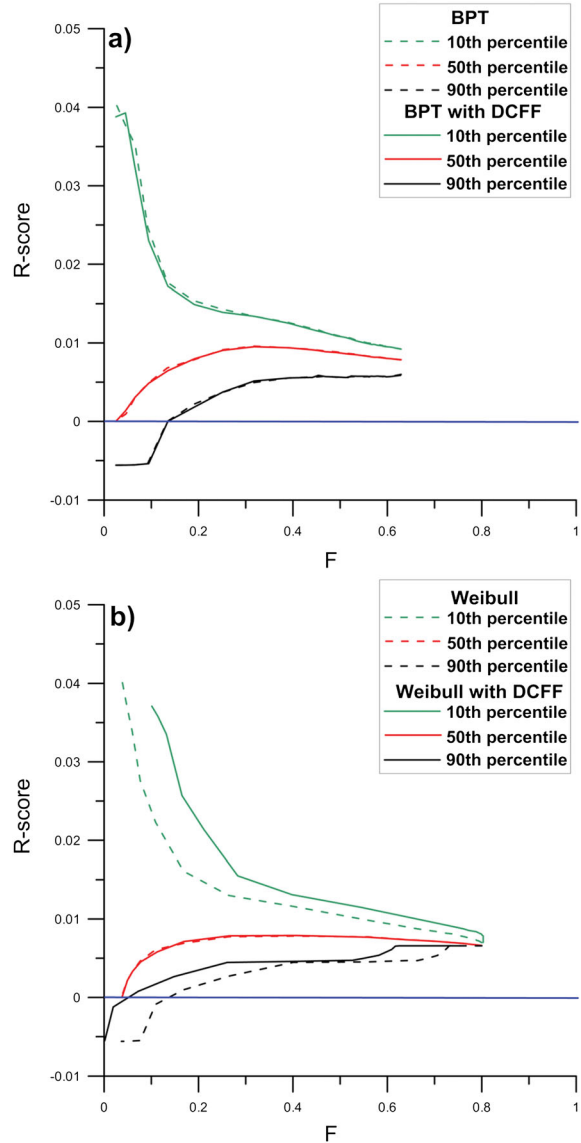


Figure 13. R-score versus the false alarm rate F for the statistical test of the two renewal models to five fault segments (1, 2, 3, 5, and 6) of the Corinth Gulf. The contribution of the stress change effect (dashed lines) is also considered. (a) For BPT model. (b) For Weibull model. The plots show the results of a Monte Carlo procedure applied to the uncertainties in the parameters of both the interevent distribution and the stress transfer algorithm. The blue line represents the trend of Poisson model.

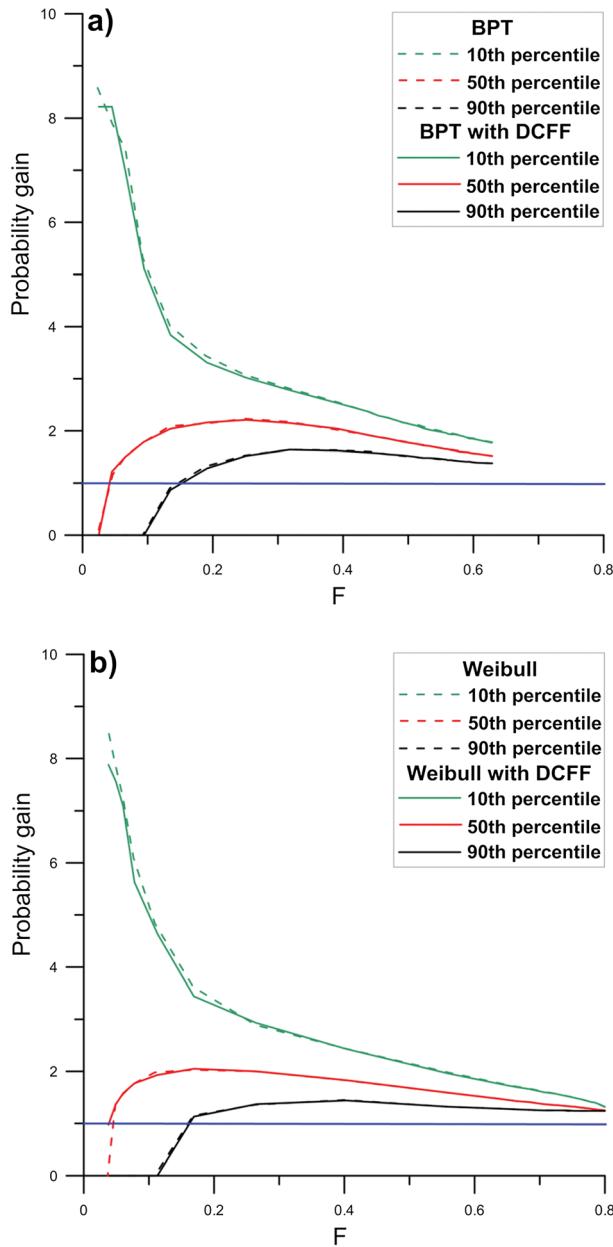


Figure 14. Probability gain versus the false alarm rate F for the statistical test of the two renewal models to five fault segments (1, 2, 3, 5, and 6) of the Corinth Gulf. The contribution of the stress change effect (dashed lines) is also considered. (a) for BPT model, (b) for Weibull model. The plots show the results of a Monte Carlo procedure applied to the uncertainties in the parameters of both the interevent distribution and the stress transfer algorithm. The blue line represents the trend of Poisson model.

5. Statistical Evaluation

[47] In the previous section, we have shown that the application of a renewal model to a sequence of characteristic earthquakes yields time-dependent probabilities for the occurrence of the next event. These probabilities can be affected also by the interaction among different segments, due to the coseismic stress change on a particular fault segment. In this section, we deal with the problem of

retrospectively evaluating the validity of the above mentioned models, by comparing the forecasts with the historical information on real earthquakes. To do so, we apply mathematical tools that have been already used in statistical seismology [Murru *et al.*, 2009] and plot the results in the Figures 12–15, also considering the effect of stress transfer, for the tenth, fiftieth, and ninetieth percentiles of the 1000 Monte Carlo procedure outcomes.

[48] An alarm-based forecast consists in defining a spatial area and future time interval within which at least

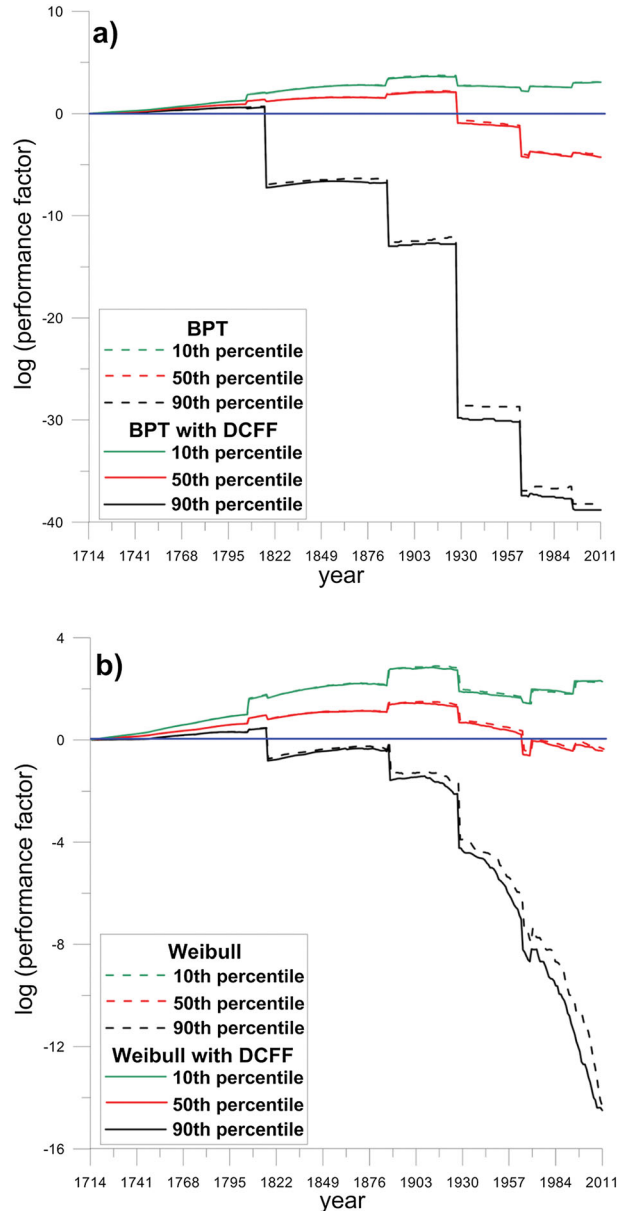


Figure 15. Log-likelihood ratio under the two renewal models, assuming the Poisson hypothesis as reference model (the whole Corinth Gulf fault system). (a) For BPT and BPT with inclusion of the static stress transfer models. (b) For Weibull and Weibull with inclusion of the static stress transfer models. The plots show the results of a Monte Carlo procedure applied to the uncertainties in the parameters of both the interevent distribution and the stress transfer algorithm. The blue line represents the trend of Poisson model.

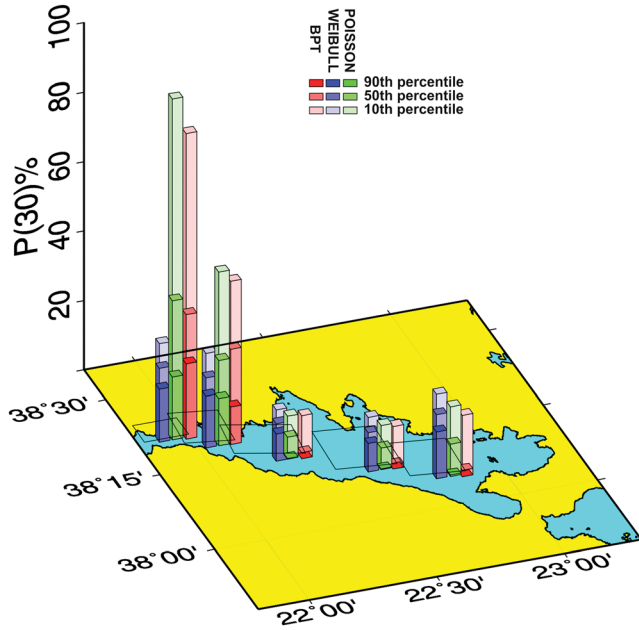


Figure 16. Probabilities for the occurrence of the next characteristic earthquake, over 30 years computed starting on 1 January 2013, on the five faults (1 - Psathopyrgos, 2 - Aigion, 3 - Eliki, 5 - Xylokastro, and 6 - Offshore Perachora) having more than one event, according to Poisson, Weibull, and BPT models.

one earthquake exceeding a certain magnitude threshold is expected to occur. In our application, an alarm is declared when the expected 1 year probability of occurrence obtained from the forecast model for any of the fault segments considered in the test exceeds a given probability threshold. Twenty-nine thresholds, ranging between $1 \cdot 10^{-8}$ and $2 \cdot 10^{-2}$, have been adopted in this study. Alarm-based forecasts are suitable for filling a binary (2×2) contingency table as shown in Table 5, where each entry corresponds to one of the four possible combinations of occurred or not-occurred and forecasted or unforecasted earthquake in each of the space-time cells. In our case, these cells are defined as a single fault segment for the duration of 1 year. The meaning of the four entries is the following:

- a –the number of successful alarms
- b –the number of false alarms
- c –the number of cells without any alarm or any earthquake
- d –the number of missed alarms.

[49] The binary contingency table, once the entries *a*, *b*, *c*, and *d* are filled with a suitably large number of observations, allows the computation of statistical indicators of the validity of the model. In this study, we apply three of these indicators: the Relative Operating Characteristic (ROC) diagram, the R-score, and the performance factor.

[50] The ROC diagram is a plot in which the *x* axis (false alarm rate) is defined as

$$F = b/(b + c) \text{ (the fraction of alarms issued where an event has not occurred)}$$

and the *y* axis (Hit rate) is defined as

$$H = a/(a + d) \text{ (the fraction of events that occur on an alarm cell).}$$

[51] The values of both *F* and *H* depend on the probability threshold adopted for giving an alarm, because this threshold affects the number of cells for which an alarm is issued. Therefore, it is a usual practice to let the alarm threshold change in order to have the number of alarms ranging from zero to the total number of cells. For the application of the statistical tools adopted in this study, we have only considered the sources that have had at least two historical events (i.e., only segments 1, 2, 3, 5 and 6). We have not considered the faults (i.e., segments 4, 7, and 8) with only one historical event as their contribution to the statistical test would be exclusively negative.

[52] Figures 12a and 12b show the ROC diagram obtained from the application of the forecast methods for both the BPT and Weibull distributions. We also plot the stress transfer effect to the data set adopted in this study. The expected trend of the ROC diagram for completely random forecasts is a straight line between point (0, 0) (no alarms given and no event forecast) to point (1, 1) of the plot (all the space-time volume occupied by forecasts and all events forecast) (blue line in Figures 12a and 12b). A point of the ROC diagram above this straight line denotes a forecast method that performs better than the time-independent Poisson hypothesis. This is the case for our application to the Corinth Gulf fault segments, except for the case of the ninetieth percentile and for $H < 0.2$ only.

[53] The R-score is defined as the number of cells in which earthquakes are successfully predicted divided by the total number of cells containing alarms minus the number of failures to predict divided by the total number of cells without any alarms:

$$R = a/(a + b) - d/(c + d)$$

[54] The R-score is still a function of the probability threshold adopted for giving an alarm, and a plot of its value can be drawn versus the fraction of false rate alarms *F*. The results of our application with the same assumptions seen for the ROC diagram are shown in Figures 13a and 13b. The expected behavior of the R-score for a plain time-independent Poisson model is a constant equal to zero (blue line in Figures 13a and 13b). All the positive values of the R-score denote a forecast method that performs better than purely randomly given forecasts, as is the case in our test, except for very low threshold values, at a 90% confidence level.

[55] The probability gain is the ratio between the conditional probability (success rate) and the unconditional probability (average occurrence rate):

$$G = a/(a + d)e/(a + b) = H \cdot e/(a + b)$$

(where $e = a + b + c + d$, is the total number of geographic cells multiplied by the number of time bins)

Table 5. Binary Contingency Table

Forecast	Observed	
	Yes	No
Yes	a	b
No	d	c

Table 6. Comparison Between Different Models^a

Model	Log R		
	Tenth	Fiftieth	Ninetieth
L = BPT, L ₀ = Poisson	3.09	-4.01	-38.2
L = BPT+ΔCFF, L ₀ = Poisson	3.05	-4.27	-38.8
L = BPT+ΔCFF, L ₀ = BPT	-0.04	-0.26	-0.06
L = Weibull, L ₀ = Poisson	2.26	-0.35	-14.4
L = Weibull+ΔCFF, L ₀ = Poisson	2.29	-0.43	-14.5
L = Weibull+ΔCFF, L ₀ = Weibull	0.03	-0.08	-0.01

^aFinal log-likelihood ratio: $\text{Log } R = \text{Log}(L) - \text{Log}(L_0)$. The values represent the tenth, fiftieth, and ninetieth percentiles of the distribution, respectively.

[56] This is again a function of the probability threshold adopted for giving an alarm. The plot of the probability gain for our application to the Corinth Gulf with the same assumptions of the previous two plots is shown in Figures 14a and 14b. Note that the expected probability gain for a plain time-independent Poisson model is a constant equal to 1 (blue line in Figures 14a and 14b). Again, our test achieves a performance better than a Poisson random forecast, except for very low threshold values at a 90% confidence level.

[57] Having analyzed alarm-based forecasts, we now consider probability-based forecasts. These consist in stating the probability of occurrence since 1714 of at least one earthquake exceeding a well-defined magnitude threshold in a well-defined spatial area and in a particular time interval. In our application, we analyze the expected 1 year probability of occurrence of a characteristic earthquake for any of the fault segments considered in the test (Figures 10–13). We use the log-likelihood ratio to compare the performance of a time-dependent forecasting model with that of the time-independent uniform Poisson model [Console, 2001].

[58] The log-likelihood of a binomial (occurrence or nonoccurrence) process under a given hypothesis is defined as:

$$\log L = \sum_{i=1}^P [c_i \log(p_i) + (1 - c_i) \log(1 - p_i)] \quad (11)$$

where: p_i is the probability associated with the i th cell in the space-time-magnitude volume, c_i is the binary value representing nonoccurrence (0) or occurrence (1) of the event in the i th cell; Note that natural logarithms are used in equation (9).

[59] The log-likelihood ratio (Log R) is the difference between the log-likelihood computed under a model to be tested (L), and that computed for a reference model (L₀):

$$\text{Log } R = \text{Log}(L) - \text{Log}(L_0) \quad (12)$$

[60] In our test, the time-independent uniform Poisson model is taken as the reference model. The models to be tested are the two renewal models and the same with stress transfer inclusion. We assume that a positive log-likelihood ratio denotes a good performance of the forecast model under test.

[61] Figures 15a and 15b show the results of the log-likelihood ratios for the entire Corinth Gulf fault system, for the above mentioned models. It clearly shows some features of the log-likelihood ratio plots:

[62] 1. During the interevent time intervals (non occurrence time), Log R is a continuous line with positive trend

when the occurrence probability under the tested model is smaller than that under the reference model, and vice versa;

[63] 2. At the occurrence time of an event, Log R changes abruptly by a positive step if the instantaneous occurrence probability under the tested model is larger than that under the reference model, and vice versa.

[64] We can see in Figures 15 that, after a fairly steady situation of better performance of the BPT and Weibull models with respect to the time independent model, the occurrence of the 22 April 1928 (*Mw*6.3) characteristic earthquake on segment 6 (*Offshore Perachora*) has made the situation less clear. At the end of the test (December 2011), while the median values show a better performance of the renewal hypothesis against the Poisson model, the latter cannot be rejected at a 90% confidence level. In Table 6, we report the final Log R values obtained at the end of the test period under various models and hypotheses considered in the study. The values shown represent the tenth, fiftieth, and ninetieth percentiles of the Monte Carlo distribution.

6. Discussion and Conclusions

[65] The characteristic earthquake hypothesis modeled by the BPT or the Weibull distributions has been tested on the system of eight along-strike adjacent normal fault segments aligned along the southern coast of the Corinth Gulf, a relatively well-monitored region in Greece. The definition of the eight segments has required a careful examination of the geological and geophysical features of the study area, along with the historical information on the earthquakes occurring in that area. At the same time, a careful judgment was necessary for the association of the historical earthquakes to each individual segment. There is some variability in the magnitude of the earthquakes assigned to the same individual segment (see Table 4). This raises the question of whether the characteristic earthquake hypothesis is applicable to this fault system. One could even suggest that the earthquake sequence observed in the latest three centuries is just a manifestation of self organized criticality. In this view, both the limits of the rupture areas and the magnitudes associated with the ruptures would come from a random process, the consequence of which would be the Gutenberg-Richter magnitude distribution.

[66] The choice of modeling the historical sequence of the 17 earthquakes that occurred since 1714 and reported in Table 1 by means of the characteristic earthquake hypothesis has required some arbitrary assumptions. One of our assumptions was to include segment 4 in the list of Table 1. This was done to bridge the gap between segments 3 and 5. Segment 4 is the smallest in the list, and thus its characteristic magnitude would be smaller than 6.0, which is the magnitude threshold of our historical catalogue. As a consequence, only one event, the 1992 magnitude 5.7 earthquake, is present in the historical sequence, while its expected recurrence time obtained from the slip rate is only 40 years. Therefore, we must consider that the list of characteristic earthquakes for segment 4 is incomplete. Addressing a relevant issue, *Sykes and Menke* [2006] in their study on time-varying probability estimates highlighted the importance of establishing that large events are not missing in historic and prehistoric (paleoseismic) records. Paying insufficient attention to such matters can lead to estimates of repeat time and coefficient

of variation that are too large, as well as to incorrect probability calculations for future events.

[67] For a comparison among the results obtained from different models (Poisson, BPT, and Weibull), Figure 16 shows the probabilities of occurrence for the next characteristic earthquake, considering the tenth, fiftieth, and ninetieth percentiles of the Monte Carlo distribution, over the future 30 years, starting on 1 January 2013, considering the information reported in Table 2 with parameter uncertainties.

[68] The results of our statistical tests show a slight superiority of the Weibull interevent time distribution in comparison with the BPT distribution. This is mainly due to the negative jumps occurring in the performance factor at the time of the 1928 (Offshore Perachora) and 1965 (Eliki) earthquakes, which affect the BPT model in more considerable way. We may recall that negative jumps in the performance factor occur when the conditional probability estimated for the occurrence of an event is smaller under the renewal model than under the Poisson time-independent model.

[69] Taking into account the large uncertainties in the parameters adopted in the physical and statistical modeling, the application to the Corinth Gulf fault system has shown that on average the renewal (time-dependent) hypothesis performs slightly better than the time-independent Poisson hypothesis. Nevertheless, the latter cannot be rejected at a 90% confidence level. This can be partly justified by the wide range of variability adopted for all the parameters involved in the model in our Monte Carlo simulations.

[70] No clear performance enhancement is achieved by the introduction of the Coulomb static stress change into the renewal model. A possible explanation for this negative result could be found in the method adopted for computing the Coulomb static stress change (ΔCFF) on the receiving faults. For earthquake probability computations, all that is typically known in advance is that the next earthquake is expected to nucleate somewhere along the concerned fault plane [Parsons, 2005]. We do not know how tectonic stress is distributed and often have no information about asperities. Under this conservative hypothesis, in the Monte Carlo simulations carried out in this study, we have drawn single values of ΔCFF from the full set of grid nodes covering the receiving fault, including those where negative values had been obtained. However, it could be reasonable postulating that the next earthquake nucleates near the peak stress change part of the fault. Thus, perhaps drawing from the stress change values above the mean would be a better choice. Incorporation of stress transfer in earthquake probability calculations can be justified in circumstances where the calculated stress change on a fault is at least 10–20 times greater than the calculated tectonic stressing rate. In such cases, the range of probability values is calculated to be altered with a high degree of confidence [Parsons, 2005].

[71] The results of the test have shown that, in spite of the good quality of the historical information, spanning a period of time longer than three centuries, the data set is not yet sufficient for a clear answer to the question of earthquake time-dependent hazard assessment. The inclusion in the model of the clock change due to coseismic static stress interaction among different segments does not lend support to this kind of physical hypothesis. While it does not lend support, it also does not provide any evidence against the model. The

modeled interactions between these segments are just too small. One of the possible reasons behind this result is that fluid flow can induce failure in these faults accepting that the latter ones might always be at a near-failure state. We are aware that we have a careful study, with an interesting and long-duration data set, that simply fails to teach us a lot. But the fact that this data set is not adequate to teach us a lot is probably a worthwhile lesson. This conclusion can probably be generalized to the application of renewal and stress-transfer models to similar cases, when a number of assumptions and large uncertainties in the relevant parameters strongly affect the reliability of the data.

Appendix A: Events Included in the Calculations of Static Stress Changes (See Table 4)

[72] **24 January 1806, Mw6.2:** From a morphotectonic analysis, *Tsimi et al.* [2007] found that the Psathopyrgos normal fault, associated with this earthquake and striking E-W, is a single fault segment 16 km long. Assuming a pure normal fault (strike = 270°, dip = 50°, rake = -90°), the seismogenic layer bounded between 5 and 13 km, and adopting the scaling laws from *Papazachos and his colleagues* [2004], a length and width of 15 and 10 km, respectively, and a coseismic slip of 0.35 m was calculated.

[73] **22 April 1928, Mw6.3:** The observed distribution of damage implies an offshore epicenter, somewhere between Perachora and Kiato [Ambraseys and Jackson, 1990]. A length of the causative offshore Perachora fault (strike = 275°, dip = 40°, rake = -80°) equal to 18 km and a width of 16 km is assumed and a coseismic slip of 0.54 m.

[74] **6 July 1965, Mw6.3:** This event is associated with the east part of Eliki fault (strike = 281°, dip = 34°, rake = -71°) with length and width both equal to 12 km. With a seismic moment of $M_0 = 1.67 \cdot 10^{18}$ N m [Baker et al., 1997], a coseismic slip of 0.351 m was estimated.

[75] **8 April 1970, Mw6.2:** For both length and width of the activated segment (strike = 265°, dip = 30°, rake = -81°) of the Xylokastro fault, 12 km was considered. With a seismic moment of $M_0 = 9.1 \cdot 10^{16}$ N m [Liotier, 1989], a coseismic slip of 0.19 m was calculated.

[76] **31 December 1975, Mw6.0:** This event is associated with a NW-SE oblique fault (strike = 316°, dip = 71°, rake = -26°, *Kiratzi et al.*, 2008]. With a fault length of 12 km, fault width of 9.5 km, and a seismic moment of $M_0 = 1.13 \cdot 10^{18}$ N m, a coseismic slip of 0.30 m was calculated.

[77] **24 February 1981, Mw6.7:** The first strong shock of this multiple sequence is considered to have moved the Skinos fault (strike = 264°, dip = 42°, rake = -80°). A fault length of 19 km, fault width equal to 15 km, which with a seismic moment of $M_0 = 8.75 \cdot 10^{18}$ N m, resulted to an average coseismic slip of 1.3 m [Hubert et al., 1996].

[78] **25 February 1981, Mw6.4:** The second 1981 event occurred on the Alephori fault (strike = 241°, dip = 44°, rake = -85°), taken to have a length of 13 km, and the same for its width, with a seismic moment of $4.0 \cdot 10^{18}$ N m, with a lower average displacement of 66 cm [Hubert et al., 1996].

[79] **4 March 1981, Mw6.3:** For modeling the 1981 event, the results from *Jackson et al.* [1982], who mapped the

surface rupture and found offsets of up to 1 m on the Kapareli fault (strike = 50°, dip = 45°, rake = -90°), and *Hubert et al.* [1996] who took mean seismic moment to be $1.9 \cdot 10^{18}$ N m for this event, were taken into account. With a fault length and width taken equal to 13 km, a coseismic slip of 0.34 m was calculated.

[80] **18 November 1992, Mw5.7:** The rupture area of the offshore of Akrata fault (strike = 270°, dip = 30°, rake = -81°) has length and width both equal to 8 km. With a seismic moment of $M_0 = 4.1 \cdot 10^{17}$ N m [*Hatzfeld et al.*, 1996], a coseismic slip of 0.19 m was calculated.

[81] **15 June 1995 Aigion earthquake, Mw6.4:** The mapped trace of the Aigion Fault onland is about 8 km long and may extend as much as 14 km if one includes its offshore trace [*Pantosti et al.*, 2004]. A rupture length equal to 16 km and a width of 10 km, as it derives from cross sections performed for the scope of the present study and based on precisely located aftershocks, and an average displacement of 0.87 m [*Bernard et al.*, 1997] were considered for the fault (strike = 277°, dip = 33°, rake = -77°) associated with the occurrence of this strong event ($M_0 = 3.4 \cdot 10^{18}$ N m).

[82] **6 June 2008, Mw6.4:** The activated fault (strike = 209°, dip = 83°, rake = 164°) has been assigned a length of 24 km and width of 12 km (from relocated data, Karakostas et al., paper in preparation), which with a seismic moment of $M_0 = 4.56 \cdot 10^{18}$ N m (<http://www.globalcmt.org/CMTsearch.html>) gives a coseismic slip of 0.49 m.

[83] **Acknowledgments.** We are grateful to the reviewers Jochen Woessner, Andy Michael, other two anonymous reviewers, and the Associate Editor for the detailed comments that were very useful for improving the manuscript. The GMT system [*Wessel and Smith*, 1998] was used to plot some of the figures. Geophysics Department Contribution number 803.

References

Ambraseys, N. N. (2009), *Earthquakes in the Eastern Mediterranean and the Middle East: A Multidisciplinary Study of 2000 Years of Seismicity*, pp. 947, Cambridge University Press, Cambridge, U.K.

Ambraseys, N. N., and J. A. Jackson (1990), Seismicity and associated strain of central Greece between 1890 and 1988, *Geophys. J. Int.*, *101*, 663–708.

Ambraseys, N. N., and J. A. Jackson (1997), Seismicity and Strain in the Gulf of Corinth (Greece) Since 1694, *J. Earthquake Eng.*, *1*(3), 433–474, doi:10.1142/S1363246997000179.

Armijo, R., B. Meyer, G. C. P. King, A. Rigo, and D. Papanastassiou (1996), Quaternary evolution of the Corinth Rift and its implications for the Late Cenozoic evolution of the Aegean, *Geophys. J. Int.*, *126*, 11–53.

Baker, C., D. Hatzfeld, H. Lyon-Caen, E. Papadimitriou, and A. Rigo (1997), Earthquake mechanisms of the Adriatic Sea and western Greece: Implications for the oceanic subduction–continental collision transition, *Geophys. J. Int.*, *131*, 559–594.

Beeler, N. M., R. W. Simpson, S. H. Hickman, and D. A. Lockner (2000), Pore fluid pressure, apparent friction, and Coulomb failure, *J. Geophys. Res.*, *105*, 25,533–25,542.

Bell, R. E., L. C. McNeill, J. M. Bull, T. J. Henstock, R. E. L. Collier, and M. R. Leeder (2009), Fault architecture, basin structure and evolution of the Gulf of Corinth Rift, central Greece, *Basin Res.*, *21*, 824–855, doi:10.1111/j.1365-2117.2009.00401.x.

Bernard, P., et al. (1997), The Ms=6.2, June 15, 1995 Aigion earthquake (Greece): Evidence for low angle normal faulting in the Corinth rift, *J. Seismol.*, *1*, 131–150, doi:10.1023/A:1009795618839.

Bernard, P., et al. (2006), Seismicity, deformation and seismic hazard in the western rift of Corinth: New insights from the Corinth Rift Laboratory (CRL), *Tectonophysics*, *426*, 7–30, doi:10.1016/j.tecto.2006.02.012.

Billiris, H., et al. (1991), Geodetic determination of tectonic deformation in central Greece from 1900 to 1988, *Nature*, *350*, 124–129.

Briole, P., A. Rigo, H. Lyon-Caen, J. C. Ruegg, K. Papazissi, C. Mitsakaki, A. Balodimos, G. Veis, D. Hatzfeld, and A. Deschamps (2000), Active deformation of the Corinth rift, Greece: Results from repeated Global Positioning surveys between 1990 and 1995, *J. Geophys. Res.*, *105*, 25,605–25,625, doi:10.1029/2000JB900148.

Brooks, M., and G. Ferentinos (1984), Tectonics and sedimentation in the Gulf of Corinth and the Zakynthos and Kefallina channels, *Tectonophysics*, *101*, 25–54, doi:10.1016/0040-1951(84)90040-4.

Catalii, F., M. Cocco, R. Console, and L. Chiaraluce (2008), Modeling seismicity rate changes during the 1997 Umbria-Marche sequence (central Italy) through a rate- and state-dependent model, *J. Geophys. Res.*, *113*, B11301, doi:10.1029/2007JB005356.

Chery, J. (2001), Core complex mechanics: From the Gulf of Corinth to the Snake Range, *Geology*, *29*, 439–442, doi:10.1130/0091-7613(2001)029<0439:CCMFTG>2.0.CO.

Clarke, P. J., D. Paradisis, O. Briole, P. C. England, B. E. Parsons, H. Billiris, G. Veis, and J.-C. Ruegg (1997), Geodetic estimate of seismic hazard in the Gulf of Korinthos, *Geophys. Res. Lett.*, *24*, 1,303–1,306, doi:10.1029/97GL01042.

Cocco, M., and J. R. Rice (2002), Pore pressure and poroelasticity effects in Coulomb stress analysis of earthquake interactions, *J. Geophys. Res.*, *107*(B2), 2030, doi:10.1029/2000JB000138.

Collier, R. E. L., D. Pantosti, G. D'Addezio, P. M. De Martini, E. Masana, and D. Sakellariou (1998), Paleoseismicity of the 1981 Corinth earthquake fault: Seismic contribution to extensional strain in central Greece and implications for seismic hazard, *J. Geophys. Res.*, *103*, 30,001–30,019, doi:10.1029/98JB02643.

Console, R. (2001), Testing earthquake forecast hypothesis, *Tectonophysics*, *338*, 261–268.

Console, R., and F. Catalii (2006), A rate-state model for aftershocks triggered by dislocation on a rectangular fault: A review and new insights, *Ann. Geophys.*, *49*(6), 1259–1273, doi:10.4401/ag-3095.

Console, R., M. Murru, G. Falcone, and F. Catalii (2008), Stress interaction effect on the occurrence probability of characteristic earthquakes in Central Apennines, *J. Geophys. Res.*, *113*, B08313, doi:10.1029/2007JB005418.

Console, R., M. Murru, and G. Falcone (2010), Probability gains of an epidemic-type aftershock sequence model in retrospective forecasting of $M \geq 5$ earthquakes in Italy, *J. Seismol.*, *14*, 9–26, doi:10.1007/s10950-009-9161-3.

Davies, R., P. England, B. Parsons, H. Billiris, D. Paradisis, and G. Veis (1997), Geodetic strain of Greece in the interval 1892–1992, *J. Geophys. Res.*, *102*, 24,571–24,588, doi:10.1029/97JB01644.

Galanopoulos, A. G. (1953), Katalog der Erdbeben in Griechenland zur die Zeit von 1879 bis 1892, *Annal. Geol. Pays Hellen.*, *5*, 115–229.

Gonzalez, A., J. B. Gomez, and A. F. Pacheco (2006), The occupation of a box as a toy model for the seismic cycle of a fault, *Am. J. Phys.*, *73*(10), 946–952. [Erratum 2007, *75*(3), 286], doi:10.1119/1.2426356.

Grunthal, G., and R. Wahlstrom (2007), A unified database of large European earthquakes, *Eos Trans. Am. Geophys. Union*, *88*(6), 69–71.

Harris, R. A. (1998), Introduction to special section: Stress triggers, stress shadows, and implications for seismic hazard, *J. Geophys. Res.*, *103*, 24,347–24,358, doi:10.1029/98JB01576.

Hatzfeld, D., G. Pedotti, P. Hatzidimitriou, and K. Makropoulos (1990), The strain pattern in the western Hellenic arc deduced from a microearthquake survey, *Geophys. J. Int.*, *101*(1), 181–202, doi:10.1111/j.1365-246X.1990.tb00767.x.

Hatzfeld, D., et al. (1996), The Galaxidi earthquake of 18 November 1992; A possible asperity within normal fault system of the Gulf of Corinth (Greece), *Bull. Seismol. Soc. Am.*, *86*(6), 1987–1991.

Hatzfeld, D., V. Karakostas, M. Ziazia, I. Kassaras, E. Papadimitriou, K. Makropoulos, N. Voulgaris, and C. Papaioannou (2000), Microseismicity and faulting geometry in the Gulf of Corinth, *Geophys. J. Int.*, *141*, 438–456, doi:10.1046/j.1365-246x.2000.00092.x.

Hubert, A., G. King, R. Armijo, B. Meyer, and D. Papanastassiou (1996), Fault re-activation, stress interaction and rupture propagation of the 1981 Corinth earthquake sequence, *Earth Planet. Sci. Lett.*, *142*, 573–585.

Jackson, J. A. (1987), Active continental deformation and regional metamorphism, *Phil. Trans. R. Soc. Lond.*, *A321*, 47–66.

Jackson, J. A., and N. J. White (1989), Normal faulting in the upper continental crust: observations from regions of active extension, *J. Struct. Geol.*, *11*, 15–36.

Jackson, J. A., J. Cagnepain, G. Houseman, G. C. P. King, P. Papadimitriou, C. Souffleris, and J. Virieux (1982), Seismicity, normal faulting and the geomorphological development of the Gulf of Corinth (Greece): The Corinth earthquakes of February and March 1981, *Earth Planet. Sci. Lett.*, *57*, 377–397.

Jackson, J., A. J. Hains, and W. E. Holt (1994), A comparison of satellite laser ranging and seismicity data in the Aegean region, *Geophys. Res. Lett.*, *21*, 2849–2852.

Kagan, Y. Y., and D. D. Jackson (1999), World-wide doublets of large shallow earthquakes, *Bull. Seismol. Soc. Am.*, *89*, 1147–1155.

Kagan, Y. Y., D. D. Jackson, and R. J. Geller (2012), Characteristic Earthquake Model, 1884–2011, *Seismol. Res. Lett.*, *83*(6), 951–953.

Karakostas, V., E. Karagianni, and P. Paradisopoulou (2012), Space–time analysis, faulting and triggering of the 2010 earthquake doublet in western

- Corinth Gulf, *Nat. Hazards*, 63, 1181–1202, doi:10.1007/s11069-012-0219-0.
- King, G. C. P., and M. Cocco (2001), Fault interaction by elastic stress changes: new clues from earthquake sequences, *Adv. Geophys.*, 44, 1–39.
- King, G. C. P., D. Oppenheimer, and F. Amelung (1994a), Block versus continuum deformation in the western United States, *Earth Planet. Sci. Lett.*, 128, 55–64.
- King, G. C. P., R. S. Stein, and J. Lin (1994b), Static stress changes and the triggering of earthquakes, *Bull. Seismol. Soc. Am.*, 84, 935–953.
- Kiratzis, A., E. Sokos, A. Ganas, G. Tselentis, C. Benetatos, Z. Roumelioti, A. Serpetsidaki, G. Andriopoulos, O. Galanis, and P. Petrou (2008), The April 2007 earthquake swarm near Lake Trichonis and implications for active tectonics in western Greece, *Tectonophysics*, 452, 51–65.
- Leeder, M. R., M. J. Seger, and C. P. Stark (1991), Sedimentation and tectonic geomorphology adjacent to major active and inactive normal faults, *J. Geol. Soc. London*, 148, 331–343.
- Lin, J., and R. S. Stein (2004), Stress triggering in thrust and subduction earthquakes and stress interaction between the southern San Andreas and nearby thrust and strike-slip faults, *J. Geophys. Res.*, 109, B02303, doi:10.1029/2003JB002607.
- Liotier, Y. (1989), *Modelisation des ondes de volume des seismes de l'arc egeen*, DEA de l' Université Joseph Fourier, Grenoble, France.
- Marinatos, S. N. (1960), Helice: A submerged town of classical Greece, *Archaeology*, 13, 186–193.
- Marsan, D., E. Prono, and A. Helmstetter (2013), Monitoring Aseismic Forcing in Fault Zones Using Earthquake Time Series, *Bull. Seismol. Soc. Am.*, 103, 169–179.
- Matthews, M. V., W. L. Ellsworth, and P. A. Reasenber (2002), A Brownian model for recurrent earthquakes, *Bull. Seismol. Soc. Am.*, 92, 2,233–2,250.
- McCann, W. R., S. P. Nishenko, L. R. Sykes, and J. Krause (1979), Seismic gaps and plate tectonics: Seismic potential for major boundaries, *Pure Appl. Geophys.*, 117, 1082–1147.
- Michael, A. J. (2005), Viscoelasticity, postseismic slip, fault interactions, and the recurrence of large earthquakes, *Bull. Seismol. Soc. Am.*, 95, 1594–1603.
- Mosca, I., R. Console, and G. D'Addezio (2012), Renewal models of seismic recurrence applied to paleoseismological and historical observations, *Tectonophysics*, 564–565, 54–67.
- Mouyaris, N., D. Papastamatiou, and C. Vita-Finzi (1992), The Helice fault?, *Terra Nova*, 4, 124–129.
- Murru, M., R. Console, and G. Falcone (2009), Real-time earthquake forecasting in Italy, *Tectonophysics*, 470(3–4), 214–223, doi:10.1016/j.tecto.2008.09.010.
- Pantosti, D., P. De Martini, I. Koukouvelas, L. Stamatopoulos, N. Palyvos, S. Pucci, F. Lemeille, and S. Pavlides (2004), Palaeoseismological investigations of the Aigion Fault (Gulf of Corinth, Greece), *Compt Rendus Geosci.*, 336, 335–342.
- Papazachos, B. C., and C. Papazachou (2003), *The Earthquakes of Greece*, pp. 286, Ziti Publishing, Thessaloniki, Greece.
- Papazachos, B. C., A. A. Kiratzis, and B. G. Karakostas (1997), Towards a homogeneous moment magnitude determination for earthquakes in Greece and the surrounding area, *Bull. Seismol. Soc. Am.*, 87, 474–483.
- Papazachos, B. C., E. M. Scordilis, D. G. Panagiotopoulos, C. B. Papazachos, and G. F. Karakaisis (2004), Global relations between seismic fault parameters and moment magnitude of earthquakes, *Bull. Geol. Soc. Greece XXXVI*, 1482–1489.
- Parsons, T. (2005), Significance of stress transfer in time-dependent earthquake probability calculations, *J. Geophys. Res.*, 109, B05304, doi:10.1029/2004JB003190.
- Parsons, T., R. Console, G. Falcone, M. Murru, and K. Yamashina (2012), Comparison of characteristic and Gutenberg-Richter models for time-dependent $M \geq 7.9$ earthquake probability in the Nankai-Tokai subduction zone, Japan, *Geophys. J. Int.*, doi:10.1111/j.1365-246X.2012.05595.x.
- Rigo, A., H. Lyon-Caen, R. Armijo, A. Deschamps, D. Hatzfeld, K. Makropoulos, P. Papadimitriou, and I. Kassaras (1996), Microseismicity study in the western part of the Gulf of Corinth (Greece): Implications for large-scale normal faulting mechanisms, *Geophys. J. Int.*, 126, 663–688.
- Roberts, G. P. (1996), Noncharacteristic normal faulting surface ruptures from the Gulf of Corinth, Greece, *J. Geophys. Res.*, 101(B11), 25,255–25,267, doi:10.1029/96JB02119.
- Roberts, S., and J. Jackson (1991), Active normal faulting in central Greece: an overview, in *The Geometry of Normal Faults*, edited by A. M. Roberts, G. Yielding, B. Freeman, pp. 125–142, *Geol. Soc. London, Spec. Publ.*, 56.
- Scharer, K. M., G. P. Biasi, R. J. Weldon II, and T. E. Fumal (2010), Quasi-periodic recurrence of large earthquakes on the southern San Andreas fault, *Geology*, 38, 555–558, doi:10.1130/G30746.1.
- Schmidt, J. F. J. (1879), *Studien über Erdbeben*, A. Georgi, Leipzig, pp. 360.
- Scholz, C. H. (2002), *The Mechanics of earthquakes and Faulting*, pp. 1–467, Cambridge University Press, Cambridge, U.K.
- Scholz, C. H. (2010), Large earthquake triggering, clustering, and the synchronization of faults, *Bull. Seismol. Soc. Am.*, 100, 901–909.
- Shimazaki, K., and T. Nakata (1980), Time-predictable recurrence model for large earthquakes, *Geophys. Res. Lett.*, 7, 279–282.
- Stefatos, A., G. Papatheodorou, G. Ferentinos, M. Leeder, and R. Collier (2002), Seismic reflection imaging of active offshore faults in the Gulf of Corinth: their seismotectonic significance, *Basin Res.*, 14, 487–502.
- Stein, R., A. Barka, and J. Dieterich (1997), Progressive failure on the North Anatolian fault since 1939 by earthquake stress triggering, *Geophys. J. Int.*, 128, 594–604.
- Sykes, L. R., and W. Menke (2006), Repeat times of large earthquakes: Implications for earthquake mechanics and long-term prediction, *Bull. Seismol. Soc. Am.*, 96, 1569–1596, doi:10.1785/0120050083.
- Taymaz, T., J. Jackson, and D. McKenzie (1991), Active tectonics of the north and central Aegean, *Geophys. J. Int.*, 106, 433–490.
- Tsimi, C., A. Ganas, N. Soulakelis, O. Kairis, and S. Valmis (2007), Morphotectonics of the Psathopyrgos active fault, western Corinth rift, central Greece, *Bull. Geol. Soc. Greece*, XXXX, Proceedings of the 11th International Congress, Athens, 13 pp.
- Utsu, T. (1972), Aftershocks and earthquake statistics (IV) - Analyses of the distribution of earthquakes in magnitude, time, and space with special consideration to clustering characteristics of earthquake occurrence (2), *J. Fac. Sci., Hokkaido Univ. Ser. VII*, 4, 1–42.
- Vere-Jones, D. (1970), Stochastic models for earthquake occurrence (with discussion), *J. Roy. Stat. Soc. Ser. B. Methodol.*, 32, 1–62.
- Vere-Jones, D. (1978), Earthquake prediction: A statistician's view, *J. Phys. Earth*, 26, 129–146.
- Weibull, W. (1951), A statistical distribution function of wide applicability, *J. Appl. Mech. - T ASME*, 18(3), 293–297.
- Wells, D. L., and K. J. Coppersmith (1994), New Empirical Relationships among Magnitude, Rupture Length, Rupture Width, Rupture Area, and Surface Displacement, *Bull. Seismol. Soc. Am.*, 84(4), 974–1002.
- Wessel, P., and W. H. F. Smith (1998), New, improved version of the Generic Mapping Tools Released, *Eos. Trans. AGU*, 79, 579.